AN EXPERIMENTAL STUDY OF THE EFFECTS OF ASYMMETRIC FUEL NOZZLES ON THE STABILITY OF TURBULENT DIFFUSION FLAMES

BY

Todd Michael Phillips

A Thesis
Submitted to the Faculty of Graduate Studies
In Partial Fulfillment of the Requirements for the Degree of

Master of Science
In
Mechanical Engineering

Department of Mechanical and Manufacturing Engineering
University of Manitoba
Winnipeg, Manitoba
Canada

THE UNIVERSITY OF MANITOBA

FACULTY OF GRADUATE STUDIES

*****

COPYRIGHT PERMISSION

AN EXPERIMENTAL STUDY OF THE EFFECTS OF ASYMMETRIC FUEL NOZZLES ON THE STABILITY OF TURBULENT DIFFUSION FLAMES

BY

Todd Michael Phillips

A Thesis/Practicum submitted to the Faculty of Graduate Studies of The University of Manitoba in partial fulfillment of the requirement of the degree

OF

MASTER OF SCIENCE

Abstract

This thesis reports some preliminary qualitative results concerning the effect of the geometry of a burner on the characteristics of turbulent jet cold and reacting flow as well as swirling and non-swirling diffusion flames. The emphasis was put particularly on the effect of asymmetric nozzle geometry on the shape and stability of turbulent jet methane flames as well as swirling methane flames.

To achieve the objectives of this study, a test rig was designed, developed and commissioned during the course of this thesis. The test rig consists mainly of an interchangeable central fuel nozzle surrounded by an annulus for swirling combustion air, as well as other components, such as flow control and flow seeding systems. Four differently shaped nozzles having similar hydraulic diameter were developed and tested. These nozzle's shapes are rectangular, circular with a contraction, square and triangular. In addition, a pipe nozzle was also used as a reference. Two types of measurements were conducted; (a) The axial mean-velocity and turbulence intensity profiles on the centre line of jet cold flow were determined by using a Laser Doppler Anemometry (LDA) and, (b) jet flame lift off and blow out as well as the overall shape and stability of swirling methane flames were obtained by using a high speed imaging system.

The main findings of this qualitative study are that asymmetric nozzles seem to improve significantly the stability of turbulent jet flames. As for swirling flames, the preliminary observations revealed that the overall flame shape is mostly dependant on swirl strength and not on nozzle geometry, particularly for high swirl numbers.

Acknowledgements

I would like to acknowledge and thank my supervisor, Dr. Birouk, for his continued invaluable guidance, help and insight throughout the life of the project. I would also like to acknowledge Dr. Tachie, Dr. Soliman and Dr. Ormiston for their advice on different aspects of the project, as well as Dr. Bartley for helping me learn how to use some equipment borrowed from his lab. As well, I am very thankful to John Finken, Paul Krueger, Irwin Penner and Kim Majury for their technical support.

I thank also Chris Iyogun, who helped me during the experimental work in the combustion laboratory. Jarrod Malenchak and Sean Clark were extremely helpful in MATLAB and other minor problems I encountered. I would finally like to thank my parents and Jaclyn Newman whose overall encouragement made each day a little easier.

Table of Contents

List of Tables

List of Figures

Chapter 1: Introduction

The demand for energy is continually increasing as industrial and residential areas keep expanding. As environmental legislation becomes stricter, the need for cleaner energy conversion systems is required. Although renewable energies, such as solar and wind power, as well as bio-fuels, are gaining much more attention, fossil fuels will likely to continue to be the primary source of energy for many decades to come. Almost all land-based and marine-based as well as aircraft and spacecraft energy conversion systems are combustion-based. There are two main modes of combustion; premixed and non-premixed. Although both combustion systems have their advantages and disadvantages, non-premixed combustion has been widely used in practice due primarily to its safe use and ease in control. This is because a diffusion (i.e. non-premixed) flame occurs at the same time as the reactants mix. This allows for better control of the size and shape of the flame, as well as prevents any flashback of the flame into the burner supply system. In practical systems, the combustion air is generally swirled around the fuel, which issues from a central pipe, to provide much better stability to the flame. The major downside of non-premixed combustion compared to its counterpart premixed is its relatively higher pollution level.

Manufacturers of non-premixed combustion energy conversion systems have two major challenges; reduce combustion emission to a minimum level while keeping high thermal efficiency. Research on non-premixed combustion contributed tremendously in improving the technology of these systems towards meeting the aforementioned objectives. However, due to the complexity of non-premixed combustion, research is still

ongoing to gain much better understanding of the complex interaction mechanisms between the turbulence of the flow field and chemistry of the flames.

Researchers across the globe working in this area created an international workshop to exchange ideas and provide new data to help advance the science of non-premixed combustion. Members of the international workshop on measurements and computation of turbulent non-premixed flames meet every two-year at the International Symposium of the Combustion Institute to discuss recent advances and the remaining challenges [1]. For instance, active members of this international body published recently an interesting article in which they reported the outstanding issues to be solved in order to improve our understanding of the swirling flows and flames in non-premixed combustion [2]. Among these challenges are (a) the understanding of the vortex breakdown and ensuing formation of a recirculation zone, (b) structure and stabilization of the recirculation zone and (c) the formation of pollutants. It was reported that resolving the aforementioned challenging research issues would require extensive measurements in well-designed burner geometries [2-3].

The research started with this project, at the University of Manitoba, is an attempt to contribute to the international effort in studying and understanding non-premixed combustion phenomenon. The primary goal of this research is to gain insight into the effects of a gas burner's geometry on the flow field structure and combustion characteristics. The literature survey presented in the next chapter (i.e. Chapter 2) revealed that although the flow structure and flame characteristics of a jet issuing from a

non-cylindrical nozzle were studied in the past, results are still inconclusive. This is basically the case for the flame lift-off and blow-out limits correlations that were developed for conventional nozzles, but have not been yet extended to include other nozzle's geometries and, thus, make them more universal. Moreover, non-premixed combustion of flames issuing from a non-cylindrical fuel nozzle surrounded by an annular swirling combustion air has not been reported in the open literature. Therefore, the specific objectives of the present work are to assess further the effects of a non-symmetrical nozzle's geometry on (i) the lift-off and blow-out of jet methane flames and, (ii) the global shape and stability of swirling diffusion methane flames.

Chapter 2: Literature Survey

This chapter excludes the analysis of the literature concerning non-premixed combustion issuing from conventional burners. A conventional burner is a burner that consists of a central cylindrical fuel nozzle surrounded by an annulus of swirling combustion air. However, some recent key references pertinent to the present study will be mentioned whenever it is needed. As the focus of this thesis is on the effects of asymmetrical nozzle's geometry on the blow-out and lift-off of jet flames, only literature pertinent to this subject is reviewed thereafter.

As mentioned above in Chapter 1, swirling diffusion flames are still less understood due to their complexity. Recently noticeable progress has been made in understanding these complex flows, thanks to the progress made in the development of laser-based measuring tools. The focus of these studies was particularly on understanding the role of swirl's strength on the overall structure of reacting flows and its impact on pollutants formation (see, for example, [2,4-8] and references cited therein). Note that in all these studies the fuel central nozzle used was cylindrical.

Recent research findings on the flow structure of a non-conventional cylindrical nozzle revealed that jets issuing from non-axisymmetric nozzles have better characteristics than their counterparts' cylindrical nozzles. So far, these studies, however, focused on the characteristics of reacting and non reacting jets issuing from asymmetric nozzles and expelling into still environments (see, for example, [9-18] and references cited therein).

For instance, Quinn [9,10] and Mi et *al.* [11] studied the effects of non-symmetrical nozzles on the centerline jet decay. Quinn [9] studied elliptical nozzles and determined that a linear relationship exists between jet decay and axial position along the centreline. The elliptical nozzle was found to entrain fluid faster than the circular nozzle and that the elliptical nozzle attained an axisymmetric shape approximately 30 diameters downstream of the nozzle exit. Mi et *al.* [11] investigated the nozzle exit geometry on the cold flow characteristics of nine differently shaped nozzles. It was found that jets with non-circular orifices had, in general, smaller jet potential cores which yields better mixing. Also, non-circular jets had a greater decay rate in the near field, but the square, cross and star-shaped jets had the same decay rate as the circular jet in the intermediate and far-field regions. It was also found that the isosceles triangular nozzle has the best mixing characteristics. In comparing their data to Quinn [9], it was found that their data did not match for similar nozzles. They attributed this to the difference in the Reynolds numbers tested in both studies. Recently Quinn [10] performed further experiments on the mixing and flow field of an isosceles triangular nozzle. The results obtained were compared to those of a circular nozzle and an equilateral triangular nozzle. Quinn's [10] results were slightly different in comparison with those of Mi et *al.* [11] as the centerline velocity decay was slightly lower. Quinn's [10] major conclusion was that the isosceles triangular nozzle has faster mixing characteristics than the circular nozzle but slower than the equilateral triangle, which refutes the work of Mi et *al.* [11]. The size of the nozzles used in these experiments may have an effect on the results. Also, the difference in Reynolds numbers employed by both group-investigators may have an effect on jet decay, something that was not determined by either group.

The characteristics of jet flames issuing from asymmetric nozzles have also received considerable attention (see, for example, [12-16] and references cited therein). The majority of these studies focused on investigating the characteristics of an elliptic jet flame (see, for example, [12-15] and references cited therein). Gollahalli et *al.* [12] studied lift-off and reattachment, concentration profiles, flame radiation, velocity profiles and temperature profiles of an elliptic flame. The elliptic nozzle was found to lift-off the flame sooner with less soot production compared with the same flame issuing from an equivalent cylindrical nozzle. They also found that the elliptic flame has a, higher temperature and nitric oxide concentration in the mid flame as compared to the circular/conventional nozzle. Prabhu and Gollahalli [13] pursued this study by using elliptical nozzles with different aspect ratios to determine the flame lift-off and reattachment, as well as concentration and temperature profiles. It was determined that the moderate elliptical nozzle (aspect ratio 3:1) had the lowest burner-rim stability and highest temperatures. Kamal and Gollahalli [14] studied the effects of Reynolds number on elliptic flames. It was determined that NO and CO emissions level off at high values of Reynolds number. Schadow et *al.* [15] studied the effects of elliptic nozzles on flames for ramjets and found that they improve combustion efficiency up to 10% due to their superior turbulent mixing. Gutmark et *al.* [16] studied the flame temperature of square, equilateral triangular, isosceles triangular and circular nozzles. They found that, overall the asymmetrical nozzles generate higher flame temperatures compared with their circular counterparts. The isosceles triangle had the highest flame's temperature; followed by the equilateral triangular while the square and circular nozzles have similar

flame temperatures. Lift-off and blow-out of jet flames issuing from asymmetrical nozzles were also studied in [17,18]. It was determined that for elliptical and circular nozzles, the blow out limits were similar for lifted flames, however, the elliptic nozzle produced more stable jet flame than that of a circular nozzle for attached flames.

Different theories have been suggested to explain the jet flame lift-off. The three most accepted theories, which were discussed in [19], are briefly summarized below.

1. The local flow velocity at the position where the laminar flame speed is a maximum matches the turbulent burning velocity of a premixed flame.
2. The local strain rates in the fluid exceed the extinction strain rate for a laminar diffusion flamelet.
3. The time available for backmixing by large-scale flow structures of hot products with fresh mixtures is less than a critical chemical time required for ignition.

The first theory was conceived by Wohl et *al.* [20] and it is the most commonly accepted theory. It has been pursued by Vanquickenborne and van Tiggelen [21]. The second theory has its origins with Peters [22] and the third with Broadwell et *al.* [23]. Vanquickenborne and van Tiggelen [21] studied the stability of methane diffusion flames. Their main finding was that diffusion flames are stabilized at a height above the burner mouth where stoichiometry is reached. They determined that the bottom, i.e. base, of the flame was a form of a premixed flame as the gas entrains air until it reaches this point. The blow off limit of a diffusion flame was found to occur at a certain lift-off

height of the flame. At this height, the turbulent burning velocity does not increase at the same rate as the local gas velocity value. Peters' [22] theory suggests that the flame will lift-off when the mixture of air and fuel in the combustion zone near the burner exit is stretched faster than the mixture can ignite itself. Kalghathi [24], in a further study, determined that the lift-off height follows a linear pattern with respect to the jet exit velocity. It was also shown that the lift-off height is independent of nozzle diameter. Furthermore, Kalghati [24] found that most hydrocarbon fuels collapse onto a single, non-dimensional lift-off height curve. Recently the explanation reported by Upatnieks et *al.* [25] contradicted the suggestions made by Kalghati [24] who stated that the lift-off height is correlated with local turbulence intensity. Upatnieks et *al.* [25] used advanced measurement techniques to determine that the laminar propagation speed at the base of the flame controls the lift-off height. Furthermore, the results dismissed the suggestions that the propagation speed of the lifted flame is governed by the turbulent burning velocity. Upatnieks et al. [25] observed that for a lifted flame, the flame is free to move and the eddies move around it. It was also determined that small turbulence eddies (less than 6.2 *mm* in diameter, which is equivalent to the jet radius at the lift off height) do not penetrate the base of the flame and pass around it. While the larger eddies (greater than 6.2 *mm*) will alter the gas velocity and cause the flame lift-off height to fluctuate. They reported that these eddies, however, do not affect the flame propagation speed and did not observe that the flame base jumped from one eddy to another which had previously been reported as a possible stabilization mechanism.

Kalghati [26] studied also the blow out stability of jet flames of various hydrocarbon fuels and stated that the blow out occurs when the change in the turbulent burning velocity cannot keep up with the local flow velocity. A linear relationship was proposed between the blow out velocity and nozzle exit diameter for hydrogen, acetylene, ethylene and methane while propane and commercial butanes had a slightly curved relationship. This correlation seems to be generally well accepted. As evidence, recent results obtained by Chao et *al.* [27] on the dilution effects on blow out limits match well with Kalghati's [26] blow out curve.

Chapter 3: Experimental Facility

3.1 Introduction

This chapter discusses the experimental test rig including the burner as well as the flow control and seeding systems. It will also outline briefly the measurement techniques employed, which are mainly a high speed camera and a TSI Laser Doppler Anemometry (LDA).

3.2. Gas Burner

The burner developed at the University of Manitoba consists of a central fuel nozzle surrounded by an annulus of air as shown in Figure 3.1. The central fuel nozzle is interchangeable so that various shapes may be used. The nozzles fit into the throat that is also the inner wall of the air annulus. The fuel pipe is inserted into the throat which is attached to the nozzle seeding chamber. The air flow enters through four axial ports that are attached through the outer chamber. The air travels between the outer and inner chambers until it reaches the top plate and enters the swirl generator after which it passes between the throat and swirl pipe. It then expels through two quarls as shown in Figure 3.1.

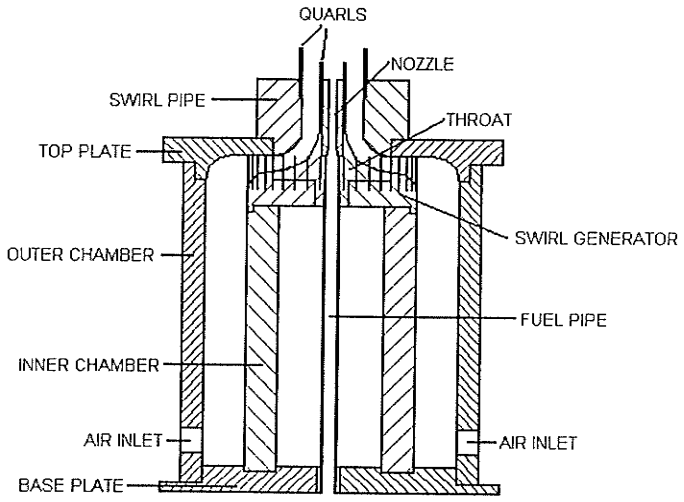

Figure 3.1: Burner design

The burner base plate, top plate and the outer and inner chambers were machined from pieces of mild steel. The swirl pipe and throat are machined from stainless steel while the fuel pipe is a stainless steel piece of extruded pipe. Plastic swirl generators were first created using a rapid prototyping machine which can create solid models from CAD images. The plastic forms were then cast out of stainless steel. This was necessary due to the complexity of machining this piece. The asymmetric nozzles were also made in this fashion while the circular nozzle was machined from a piece of stainless steel. The quarls were made from quartz tube. Their purpose was to lift slightly the flame from the nozzle throat to avoid any metal melting as the quartz can withstand much greater temperatures, up to 1740 K.

The burner outer and inner chambers have diameters of 152.4 mm and 101.6 mm, respectively, as can be seen in Figure 3.2. The flow enters the space between the chambers through four circular injection points.

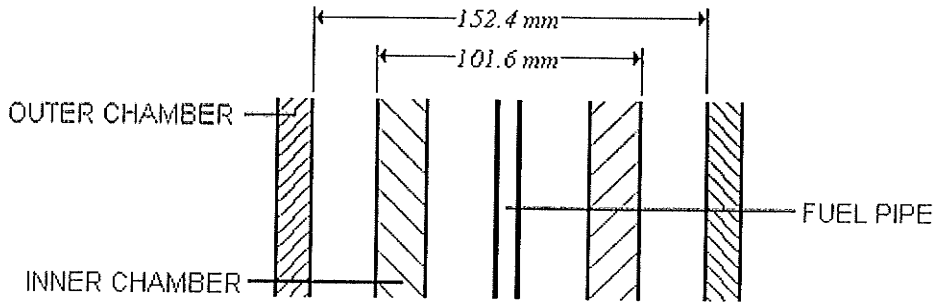

Figure 3.2: Bottom section of burner

The air travels vertically upward through the gap between the walls of the inner and outer chambers and then accelerates in the swirl generator which has a space of 10 *mm* between itself and the top plate as shown in Figure 3.3

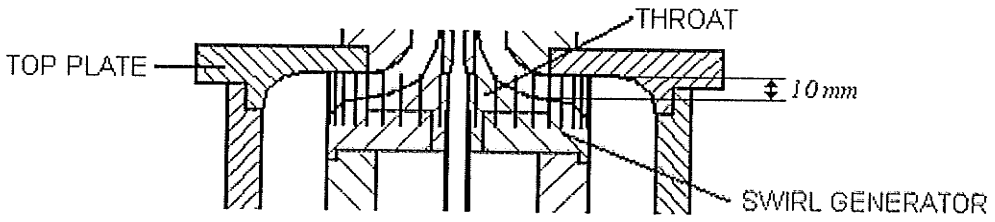

Figure 3.3 Middle section of burner

The air then expels through the exit annulus which has an inside and outside diameters of 14.9 *mm* and 36.6 *mm,* respectively, as seen in Figure 3.4.

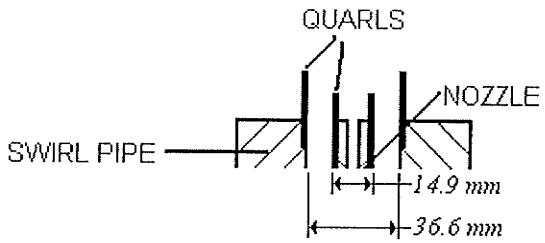

Figure 3.4: Burner exit

The fuel pipe extends well below that seen in Figure 3.5 and has a length/diameter ratio of 150, which is sufficiently long to allow for the flow to develop. The fuel pipe has an inside diameter of 7.13 *mm*. There is a transition region at the start of the nozzle which is 17 *mm* in length that transforms the passage from the circular diameter of 7.13 *mm* to whichever shape of asymmetric nozzle. The cross section of the nozzle is constant for the remaining 30 *mm* up to its tip.

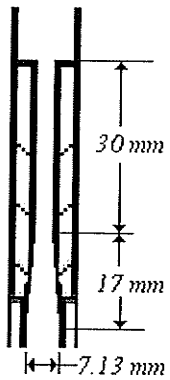

Figure 3.5: Nozzle contraction

An air annulus having a 14.9 *mm* and 36.6 *mm* inner and outer diameter, respectively, was deemed to be adequate for the type of experiments to be performed by using the current design of the burner. The fuel pipe size was chosen based on the smallest diameter that could easily be manufactured in order to conserve fuel. The swirl generation method was chosen so that if the size of annulus needed to be altered, only the swirl pipe and outer quarl would have to be modified and not the expensive swirl generator. The four swirl generators developed here are presented in Figures 3.6a through 3d and their corresponding theoretical swirl numbers, which are determined based on the formula given in [29], are tabulated in table 3.1. Figure 3.7 shows the four different nozzles developed in this study.

Table 3.1: Swirl Numbers

Swirl Vane Angle	Swirl Number
0	0
25	0.31
50	0.79
60	1.15

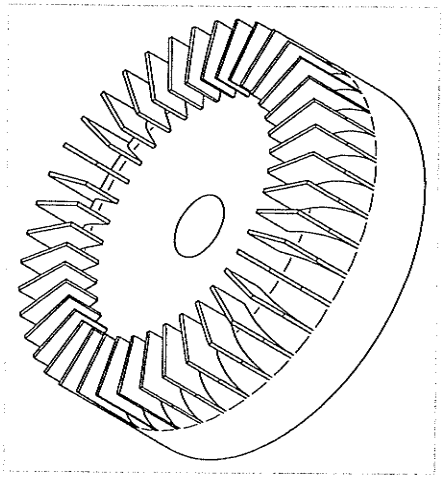

Figure 3.6a: Zero swirl angle

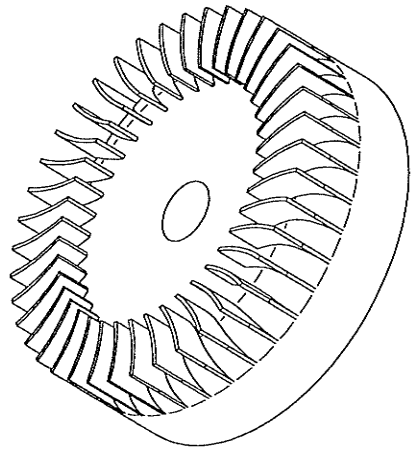

Figure 3.6b: 25 degree swirl angle

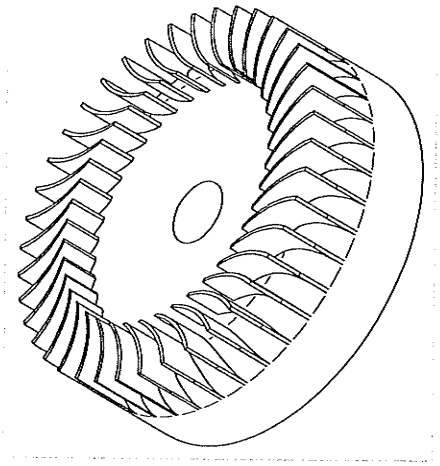

Figure 3.6c: 50 degree swirl angle

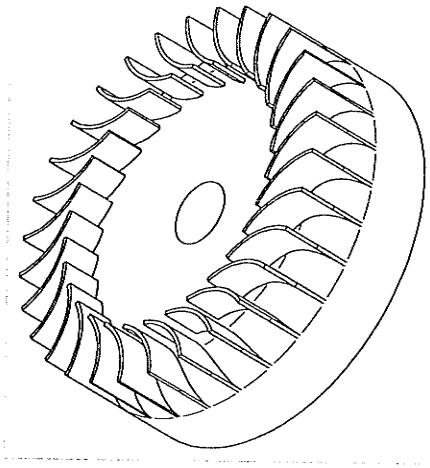

Figure 3.6d: 60 degree swirl angle

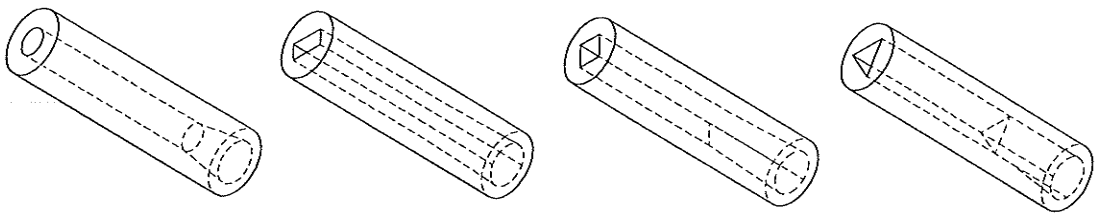

Figure 3.7: Asymmetric nozzle shapes

3.3 Flow Control System

The flow system uses compressed gases, which are controlled through a series of flowmeters and regulators. The fuel used in this experiment is a grade 2.0 methane that has a purity of 99%. It was stored in a compressed canister. The pressure was regulated by a two stage Prostar regulator and then passes through a Matheson FM-1050 series flowmeter. The regulator had an outlet pressure range of 0 – 200 *psi* while a pressure gauge installed beside the flowmeter, which had an operating range of 0 – 60 *psi,* gave an accurate reading of the pressure inside the flowmeter. The flowmeter was designed to have interchangeable tubes so that a variety of flow rates would be used. In the present experiment two tubes were used; i.e. the low flow tube had a range of 1.26 to 22.6 *LPM* of methane (0.88 to 16 LPM of air) while the high flow tube had a range of 3.51 to 59.3 *LPM* of methane (2.4 to 44 LPM of air). The flowmeter had a 6 turn utility valve at the outlet to control the flow within 1% full scale accuracy. Most of our experiments were run at a pressure of 30 *psi* in the flowmeter. The flowmeter was calibrated at atmospheric pressure, therefore, a correction factor must be used when running at higher pressures, which is given as

$$Q_{act} = Q_{read}\sqrt{P_{act}/P_{atm}} \qquad (3.1)$$

where Q_{act} is the actual flow rate, Q_{read} is the flow rate read from the flowmeter, P_{act} was the pressure in the flow meter and P_{atm} was the room atmospheric pressure. The gaseous flow rate in the central nozzle was varied to achieve a fuel velocity ranging between 2.03 *m/s* and 94.45 *m/s* (or between 1.42 *m/s* and 70.08 *m/s* for air flow). The accuracy of the flowmeter was ±1% full scale.

The air was supplied by the University of Manitoba's compressed air system. The inlet maximum pressure was 90 *psi*. The experiment air was regulated by a one-stage Prostar regulator having an operating range between 0 and 200 *psi*. A 0 – 60 *psi* gauge was employed to ensure greater accuracy. The flow was controlled by using a Brooks Model 1000 Flowmeter which has a range of 159 *LPM* to 1589 *LPM* at 30 *psi*, with an accuracy of ±1% of the full scale. A Cole-Parmer acrylic flowmeter for low velocity air flow, which is capable of a flow range between 30 to 280 *LPM* at standard conditions, was installed in parallel with the Brooks flow meter. The maximum air flow attainable from the University compressed air line was 600 *LPM* at 30 psi. The airflow velocity range achievable by using these two flowmeters ranges between 1 *m/s* and 11.41 *m/s*. The flow system had a valve connecting the air and fuel line in order to enable using air instead of gas fuel. Note that all the three flowmeters had safety valves that open up if the pressure reaches an amount that is higher than the flowmeter tubes can withstand. A schematic of the flow control system is displayed in Figure 3.8.

The flowmeters were supplied with calibration charts from the manufacturers. They were also checked using a wet test meter and the results matched very well. After LDA measurements were taken, the average velocity at the nozzle exit was also determined from the flow field. This was used with the cross sectional area to determine the flow rate. This flow rate also matched very closely with the manufacturers sheets.

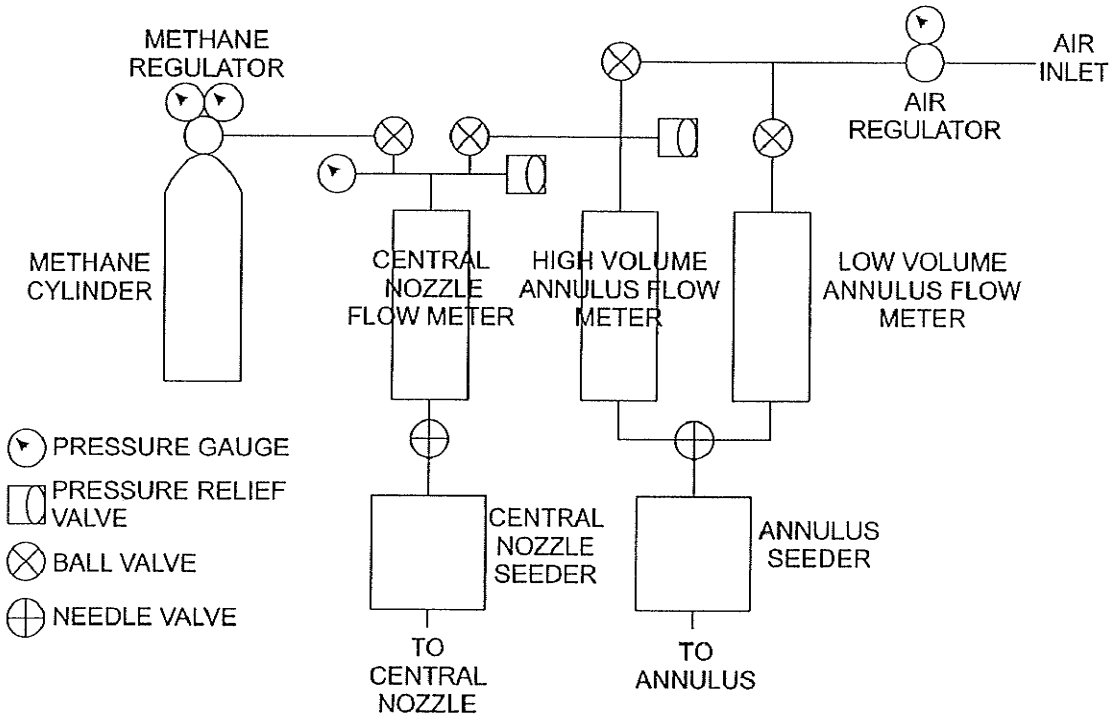

Figure 3.8: Schematic of flow control system

3.4 Flow Seeding System

The seeding system was used to seed the gas flow. These particles are necessary for the LDA system to measure the flow velocity, which is based on the scattering light by the flow (see section 3.4.2 for more details about the operating principles of LDA). The seeding system consists of two chambers in which particles can be deposited in and then picked up by the flow upstream the flow control unit. There is one seeder for the annulus of air flow and another for the central fuel nozzle. The chambers are cylinders made from mild steel and have a welded plate on the bottom and a welded flange on the top. A top plate was then bolted to the flange. Three holes were machined in the top for the air or fuel inlet/outlet and particles supply. The inlet tube enters into the seeders and is

positioned approximately 1 *cm* from the bottom of the chamber for the large seeder (for the annulus of air) and approximately 1 *mm* for the small seeder (for the central nozzle). The seeding particles used were titanium oxide with a mean diameter of 1 μm. Titanium oxide particles can survive in high temperature environment. It is important to mention that the Titanium oxide particles must be kept very dry as moisture can cause them to bond together rendering them useless.

3.5 Measurement Techniques

The measurement techniques employed were decided based on the type of data needed. For the flame lift off height and the flame length, a high speed digital video camera was used whereas LDA, which is a non-intrusive technique, was used for flow velocity measurements.

3.5.1 Imaging Technique

The camera used is a MotionScope PCI 8000S high speed camera. The optimum recording rate was found to be 60 frames per second with a shutter speed of 1/60 *s*. A ruler was first placed over the burner, as shown in Figure 3.9, and then the height of a pixel was then calculated. 1948 instantaneous images of the flame for each set of conditions were then taken and analyzed using an in-house MATLAB code. The lift-off height of all 1948 flames was averaged to determine the height. The MATLAB code calculated the lift off of each flame by using the brightness of each pixel. MATLAB code assigns each pixel a brightness level from 0 to 256 with 0 being black and 256 being

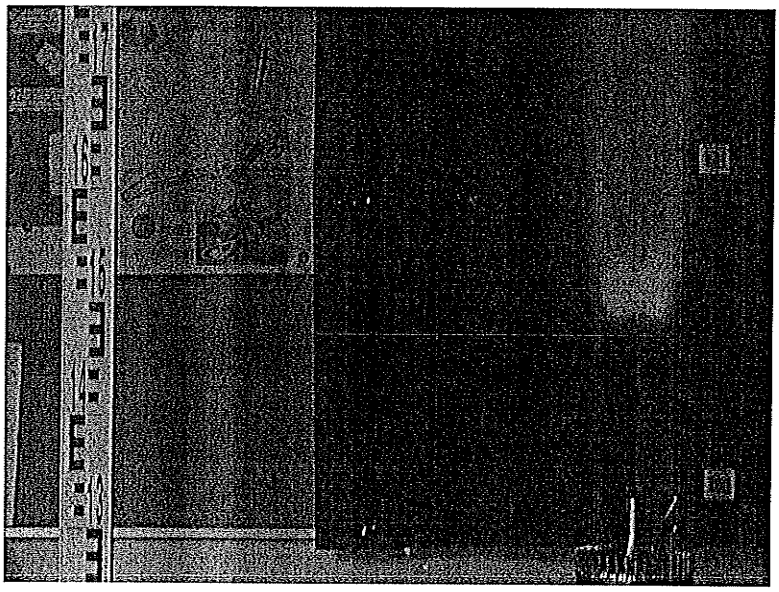

Figure 3.9: Digital picture of flame lift-off

white. By analyzing individual frames, the flame was determined to exist in regions where the brightness was 30 or higher. This allowed for background brightness to be neglected while allowing the flame location to be accurate within two or three pixels, which corresponds to about 1 *mm*. Figure 3.10 shows a typical frames for the rectangular nozzle.

The same set of images, used for determining the liftoff, were used to determine the flame length (height) using the same technique. However, as the determination of the flame length required a larger camera field of view because of the flame tip was found to fluctuate. Since the number of pixels remained constant, the error was therefore increased to $\pm$ 2 *mm*.

Figure 3.10: Flame lift off height of the rectangular nozzle

3.5.2 Laser Doppler Anemometry (LDA)

A schematic of the LDA set-up used in this thesis is shown in Figure 3.11. An Innova 70C series Argon-Ion laser generates a fixed frequency (green) light having a wavelength of 514.5 *nm*. The same beam is then split into two beams with equal intensity and frequency. These beams travel through a fiber optic cable to a transmitter which uses a lens to focus the two beams and intersects them at a 363 *mm* distance downstream of the lens. The focal point is known as the probe volume. The latter consists of a set of bright and dark fringes. As a particle passes through a certain number of bright fringes, it scatters light which is then collected by the receiving optics which is then transformed into electrical signals by a Photo Detector Module 1000(PDM 1000). Thereafter the signal passes into the TSI Flow Size Analyzer 4000 (FSA 4000) signal processor (see

Figure 3.11 below) where the FSA 4000 determines the frequency of the particle at which it crossed the set of bright fringes in the probe volume. This frequency is known as the Doppler frequency, f_D. Because the fringe spacing, δ_f, is a constant value and geometrically known, the FSA 4000 can determine the particle's velocity as $u = \delta_f f_D$. More details of this technique can be found in [30].

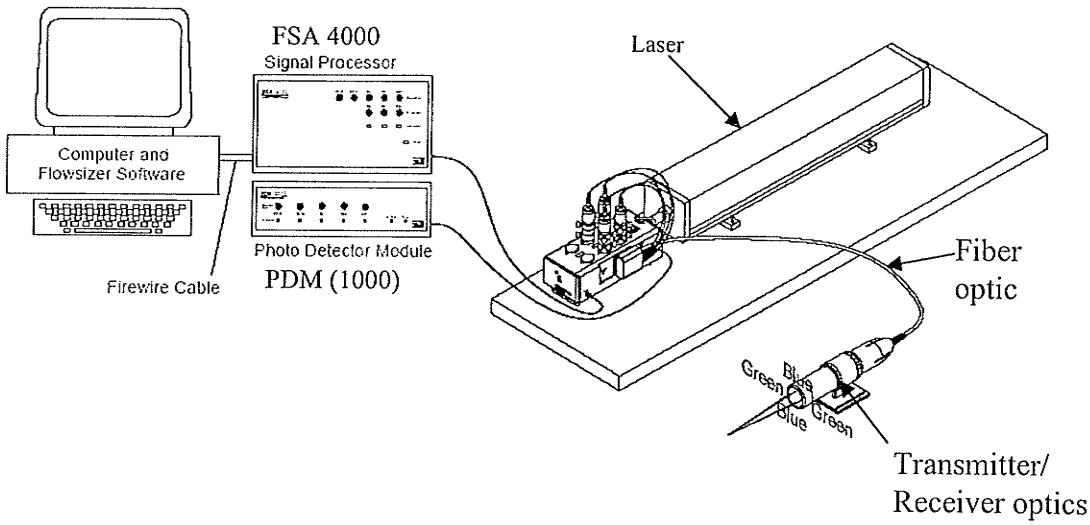

Figure 3.11: Schematic of LDA set-up [30]

Chapter 4: Results and Discussion

4.1. Introduction

The main objective of the present study was to assess the effect of a fuel nozzle geometry on the characteristics of a jet cold flow as well as a turbulent jet methane flame and swirling methane flame. For the 'cold' jet flow, the axial centerline profiles of the mean velocity and its corresponding fluctuating component were measured by using a 1D Laser Doppler Anemometry (LDA). For the jet methane flame, the emphasis was put particularly on determining flame lift-off and flame length. Finally, for the swirling diffusion methane flame, the focus was on determining the flame blow out limits (i.e. stability). Asymmetrical rectangular, square and triangular nozzles as well as a conventional (pipe) nozzle were tested in this study. In addition, a contracted circular nozzle was also tested, but only for flames. Schematic diagrams of these nozzles are shown in Figure 4.1. The same figure shows also the LDA measurement plane, which is basically through the centerline of each nozzle. This figure shows that the contracted circular and pipe nozzles have similar exit cross section; however, the circular nozzle has a contracted cross section prior to its exit area as presented in Chapter 3.

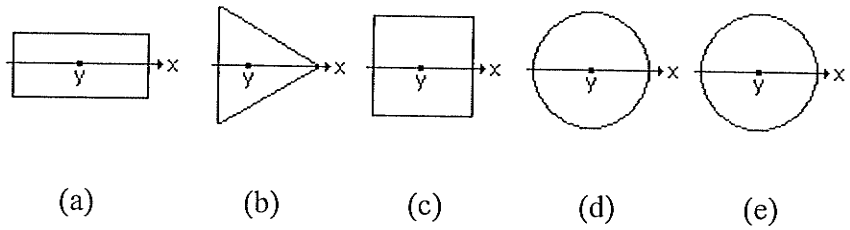

Figure 4.1: LDA measurement planes of the (a) rectangular, (b) triangular, (c) square, (d) contracted circular, and (e) conventional pipe nozzles

4.2. Jet 'Cold' Flow Characterization

The asymmetrical nozzles tested were the rectangular, square and triangular. In addition, a conventional pipe nozzle was also tested for reference. Only one cross section, which is the axial centreline plane, of each nozzle was characterized as sketched schematically in Figure 4.1. The nearest velocity measurement location was 3 *mm* downstream of the nozzle exit and the furthest was 200 *mm*. All these measurements were taken at a fixed Reynolds number Re ~16000, which corresponds to an average exit velocity of 65 *m/s*. The average exit velocity was determined by using the volumetric flow rate at the exit of each nozzle. This particular velocity was chosen as an attempt to relate the LDA measurements to the flame lift-off data.

4.2.1. Jet flow mean-velocity profiles

The axial centreline mean velocity profiles for the four nozzles above are presented at four different locations downstream of the nozzle exit, which are 3 mm, 18 mm, 53 mm and 103 mm. As shown in Figures 4.2 through 4.5 below, the maximum velocity occurs always at the central line of the measurement plane of each nozzle. In addition, Figures

4.2 and 4.3 show that the rectangular nozzle has the lowest maximum mean velocity whereas the pipe has a slightly higher centreline velocity followed by that of the square and triangular nozzles. At the nearest measurement plane, that is y = 3 *mm*, the asymmetric nozzles have almost flat mean-velocity profiles while the pipe has a smoother parabolic profile. Away from this location, the flatness of the mean-velocity profiles for the asymmetrical nozzles tends to progressively become more parabolic and resemble that of the pipe as shown in Figures 4.3 through 4.5. Contrary to the rest of the asymmetrical nozzles, the rectangular one has a slow transition from flat to parabolic mean-velocity profiles as demonstrated in the figures below. In addition, Figures 4.2 and 4.3 show that relatively near the exit location, the triangular nozzle has the highest centreline axial mean-velocity followed by the square, pipe and the rectangular. Further away from the nozzle exit, as demonstrated in Figures 4.4 and 4.5, the pipe centreline axial mean-velocity becomes the highest followed by square and rectangular which have almost similar profiles, and then the rectangular nozzle which has the lowest velocity. This suggests that the pipe nozzle has slower velocity decay than that of the asymmetric nozzles. This will be discussed in the next section. Furthermore, as shown in Figures 4.4 and 4.5, the mean-velocity profiles of all the nozzles are nearly identical in shape in the far field. This implies that the effect of the nozzle shape on the jet flow mean-velocity profiles is more significant in the region near the nozzle exit and becomes insignificant further away.

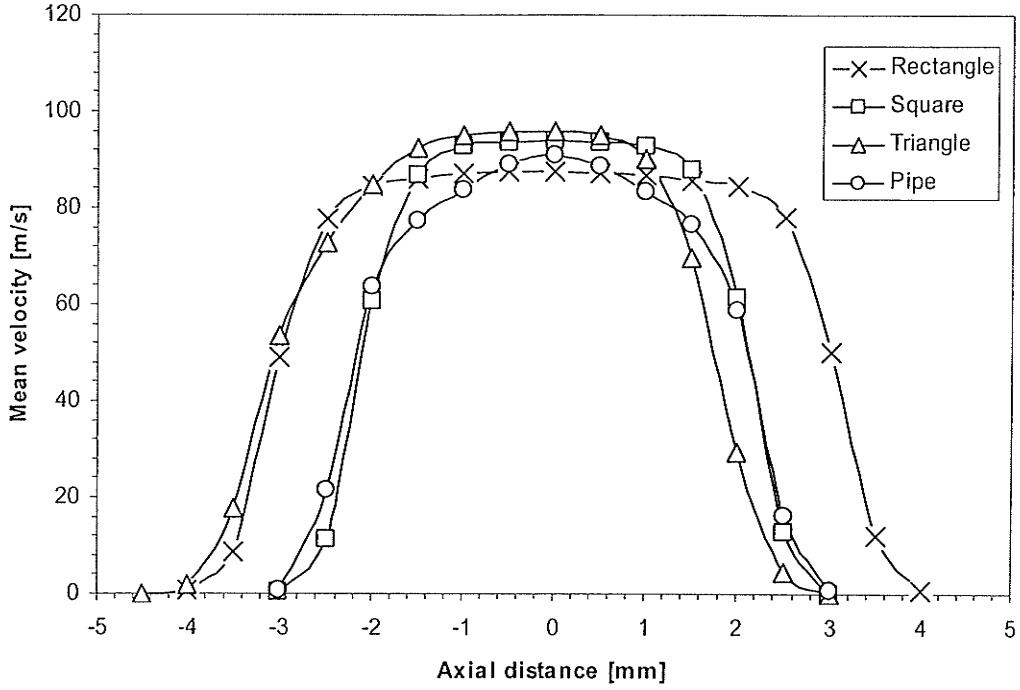

Figure 4.2: Mean-velocity profiles at y = 3 *mm*

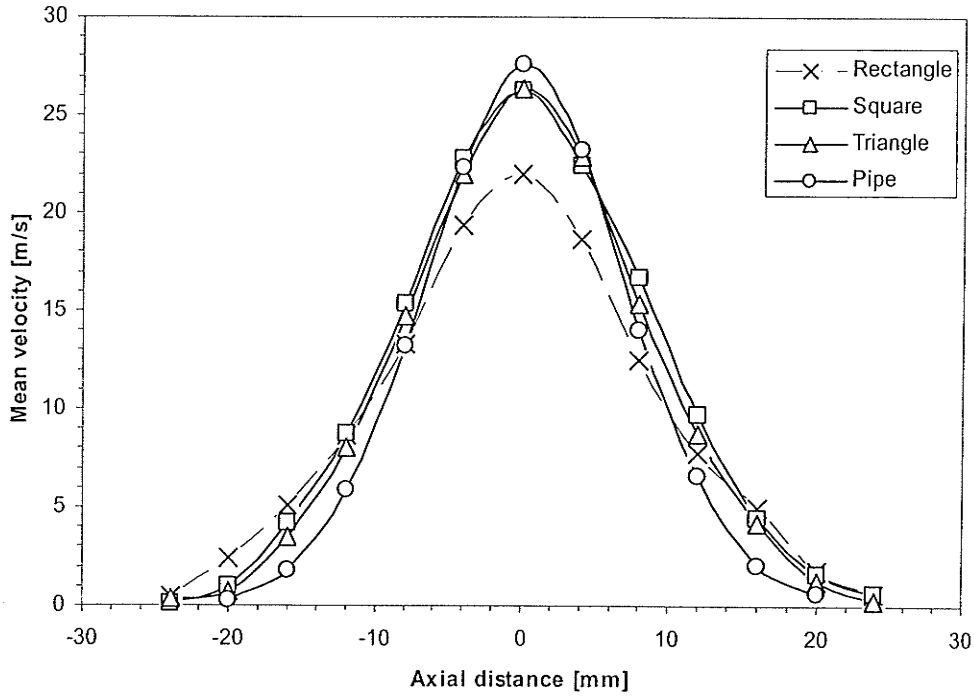

Figure 4.3: Mean-velocity profiles at y = 18 *mm*

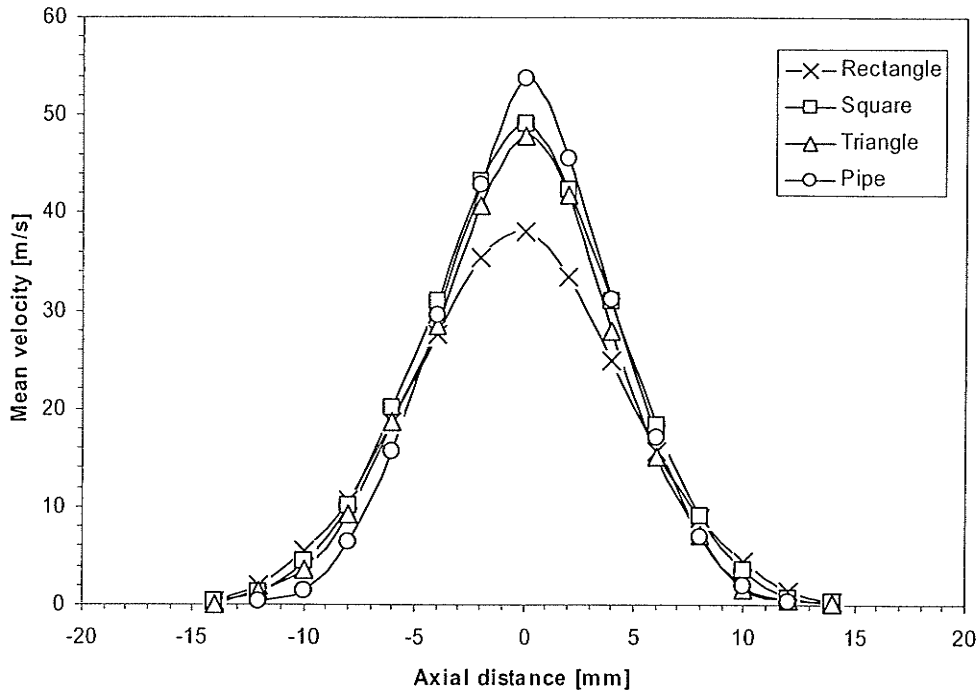

Figure 4.4: Mean-velocity profiles at y = 53 *mm*

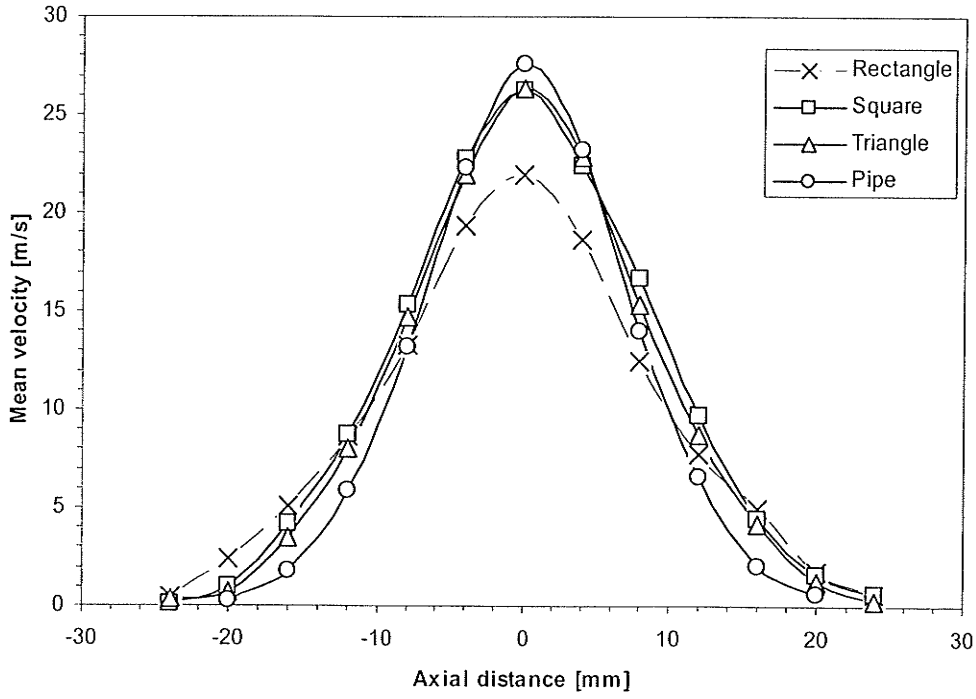

Figure 4.5: Mean-velocity profiles at y = 103 *mm*

4.2.2 Centreline jet decay

The centerline jet decay for the asymmetric nozzles as well as the pipe is shown in Figure 4.6 where U_{max} is the maximum value of the jet streamwise mean velocity and U_{cl} is the jet centerline mean velocity at any axial streamwise position. Recall that the coordinate y is the axial streamwise direction of the flow and D_e is the equivalent diameter of the nozzle exit area. The jet flow Reynolds numbers employed in both the present study and that of Mi et *al.* [11] are approximately the same. The comparison presented in Figure 4.6 shows that the results of Mi et *al.* [11] for a non-contracted circular nozzle has the slowest jet decay, and the isosceles triangular nozzle with a sharp contraction has the fastest jet decay. The same figure shows that in the present study the rectangular nozzle has the fastest jet decay, which slightly lower than that of the isosceles triangular nozzle of Mi et al. [11], followed by the triangular and square nozzles and finally the pipe, which has the slowest jet decay.

The triangular nozzle of Mi et *al.* [11] seems to have a higher jet decay compared to its counterpart used in the present study and this may be explained by the fact that their triangular nozzle has much sharper edges. Sharp edges may induce more turbulence which yields faster jet decay. It is also noticeable in the same figure that the pipe used in the present study has nearly the same jet decay as that of Mi et *al.* [11]. Faster jet decay implies higher entrainment which leads to higher mixing rates.

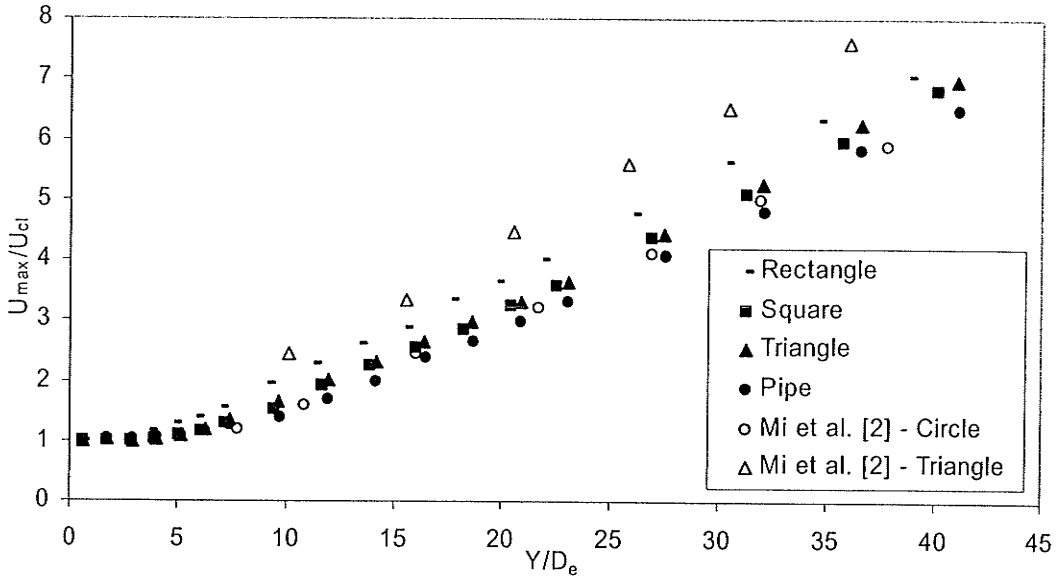

Figure 4.6: Centerline jet decay for a given R_e

The linear portion of Figure 4.6, i.e. starting from around $y/D_e \geq 7$, can be represented by the equation 4.1 reported in [9]

$$U_{\max} / U_{cl} = K_u \left(Y / D_e + C_u \right) \tag{4.1}$$

where K_u and C_u are constants which are tabulated in Table 4.1 for each nozzle tested in the present study. The values of these constants found by Quinn [9] for the sharp edge elliptical and circular nozzles as well as the contoured circular nozzle are also given in Table 4.1. The constant K_u is the slope of the jet decay; therefore, a larger value of this constant indicates faster jet decay. The constant C_u is the value at which the jet decay would cross the abscissa if it were extended and consequently, a higher value means that the jet decay starts closer to the nozzle exit. Table 4.1 shows that the results of the present

study are in good agreement with those of Quinn [9]. The asymmetric nozzles have a slightly faster jet decay as indicated by higher value of K_u. Also, the centreline jet decay for the asymmetrical nozzles starts closer to the nozzle as indicated by the higher value of C_u. The slopes are quite similar even though there is a small variation from nozzle to another. The most noticeable observation is that jet decay for the rectangular nozzle starts much earlier than any of the other nozzles.

Table 4.1: Linear constants of jet decay from equation 4.1

Nozzle	K_u	C_u	Range
Elliptic (Sharp Edge) – Quinn [25]	0.202	0.421	$7.6 \leq y/D_e \leq 61.7$
Circle (Sharp Edge) – Quinn [25]	0.202	-1.745	$8.5 \leq y/D_e \leq 63.0$
Circle (Contoured) – Quinn [25]	0.151	-1.859	$8.5 \leq y/D_e \leq 63.0$
Pipe – Present Work	0.164	-0.341	$9.66 \leq y/D_e \leq 41.12$
Rectangle – Present Work	0.173	0.280	$9.13 \leq y/D_e \leq 38.85$
Triangle – Present Work	0.170	-0.133	$9.64 \leq y/D_e \leq 41.03$
Square – Present Work	0.170	-0.158	$9.43 \leq y/D_e \leq 40.13$

In the present study we also tried to characterize the jet decay by fourth order polynomials as can be seen in Figure 4.7. The individual polynomial fits for each nozzle are tabulated in Table 4.2. In determining the polynomial equation for each nozzle, the value of U_{max}/U_{cl} was artificially set to 1 at $Y/D_e = 0$, as the maximum velocity was assumed to be at the nozzle exit. This method is more complex but it has the distinct advantage of being extremely accurate over the entire flow field. The results fit very well

with nearly every data point in the figure. Moreover, the polynomial fits can capture the near flow field region as opposed to linear approximations.

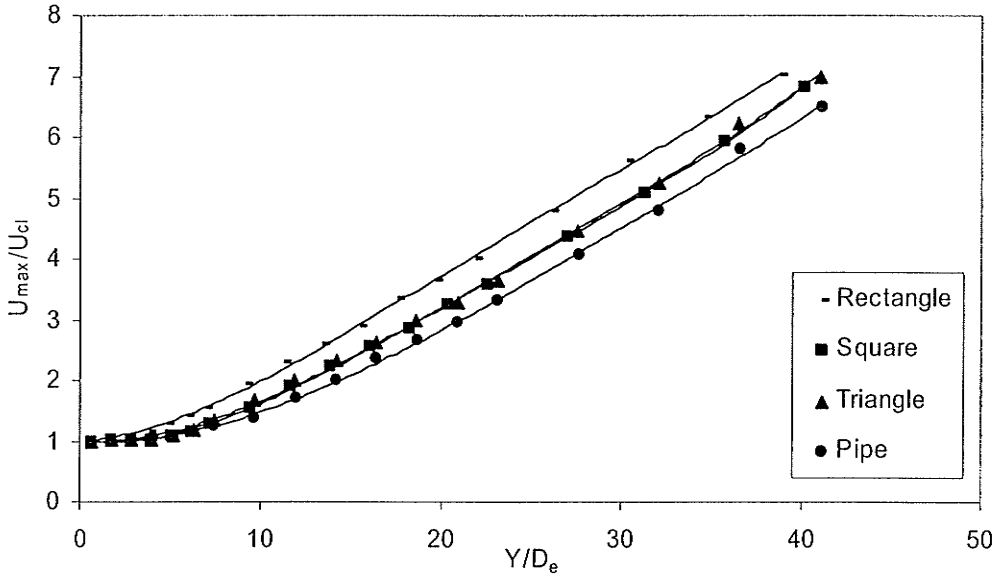

Figure 4.7: Centerline decay at Re ~ 19,000 with polynomial trend lines

Table 4.2: Fourth order polynomials jet decay

Rectangle
$U_{max}/U_{cl} = 3.34\times10^{-6}(Y/D_e)^4 - 3.25\times10^{-4}(Y/D_e)^3 + 1.12\times10^{-2}(Y/D_e)^2 + 1.65\times10^{-2}(Y/D_e) + 1.00$
Square
$U_{max}/U_{cl} = 4.08\times10^{-6}(Y/D_e)^4 - 3.83\times10^{-4}(Y/D_e)^3 + 1.34\times10^{-2}(Y/D_e)^2 + 3.69\times10^{-2}(Y/D_e) + 1.00$
Triangle
$U_{max}/U_{cl} = 2.95\times10^{-6}(Y/D_e)^4 - 2.94\times10^{-4}(Y/D_e)^3 + 1.11\times10^{-2}(Y/D_e)^2 + 1.90\times10^{-2}(Y/D_e) + 1.00$
Pipe
$U_{max}/U_{clx} = 1.32\times10^{-6}(Y/D_e)^4 - 1.66\times10^{-4}(Y/D_e)^3 + 8.35\times10^{-3}(Y/D_e)^2 + 1.98\times10^{-2}(Y/D_e) + 1.00$

4.2.3 Jet flow turbulence intensity (rms) profiles

Turbulence intensity profiles which correspond to the mean-velocity profiles presented in Figures 4.2 through 4.5 were also measured at the same streamwise locations. Turbulence intensity profiles for the four tested nozzles near the nozzle exit, i.e. at y = 3 *mm*, are shown in Figure 4.8. This figure shows that the highest rms occurs where the jet entrains the ambient air which is known as the jet boundary. The rectangular nozzle has the highest maximum turbulence intensities, which occur at $r = \pm 3$ *mm* from the centreline and were about the same strength as the apex side of the triangular nozzle. The triangular nozzle's profile was taken from the center of a flat side to the apex of the other two sides where the apex side was the negative radial positions and the flat side was the positive radial positions. The square nozzle had the next highest turbulence intensities and the pipe had the smallest. If the turbulence intensity were correlated with mixing, then these results suggest that the asymmetric nozzles had a better mixing than the pipe near the nozzle exit (i.e. in the near field).

However, away from the nozzle exit, that is at y = 18 *mm*, y = 53 *mm* and y = 103 *mm* the intensity profiles are shown in Figures 4.9, 4.10 and 4.11, respectively. Figure 4.9 shows that the turbulence intensity of the square nozzle surpasses the triangular and rectangular nozzles at y = 18 *mm* while the turbulence intensity for the pipe remains the lowest. Further downstream of the nozzle, i.e. from approximately y = 53 *mm*, the turbulence intensity profiles for the four tested nozzles tend to become smooth and parabolic though the rms velocity profiles have two small peaks near the centreline. This was observed for all nozzles and these peaks vanished at farther distances and the profiles become

completely parabolic. The main conclusion from these figures is that the asymmetric nozzles have an increased mixing in the jet boundary near the nozzle exit, but this fades quickly as the flow moves away from the nozzle exit.

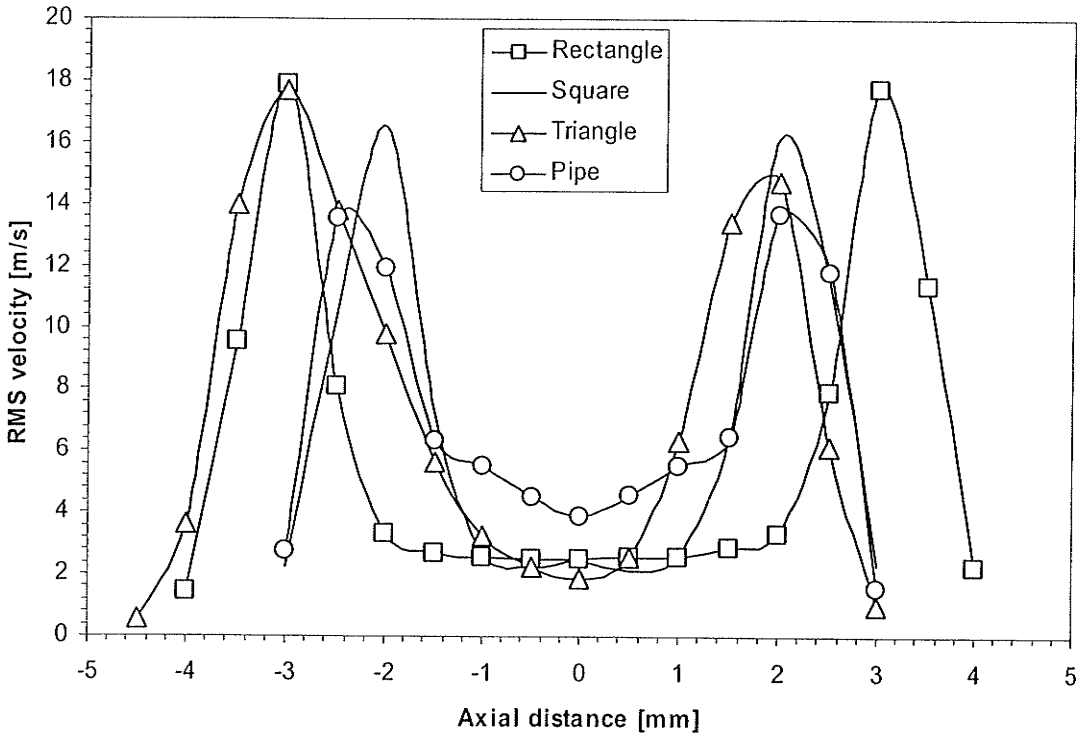

Figure 4.8: RMS velocity profiles at y = 3 *mm*

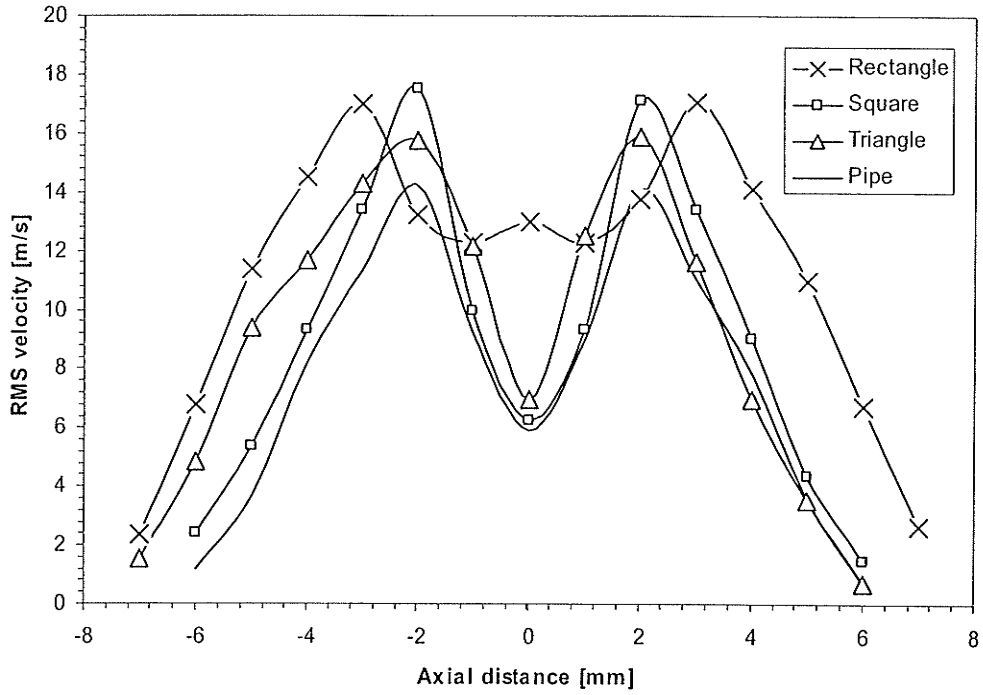

Figure 4.9: RMS velocity profiles at y = 18 *mm*

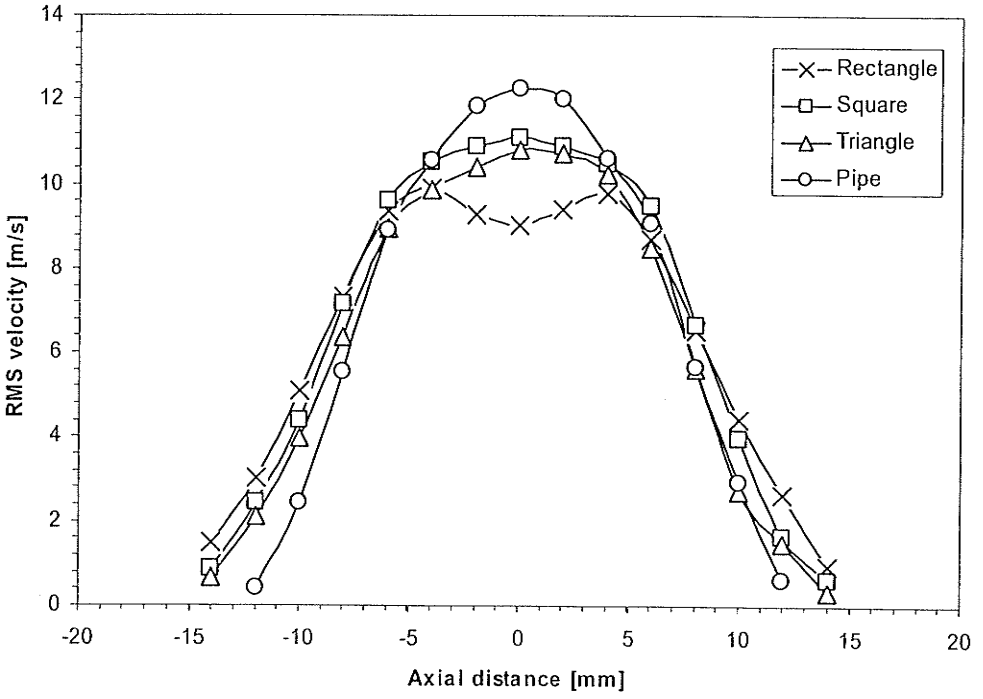

Figure 4.10: RMS velocity profiles at y = 53 *mm*

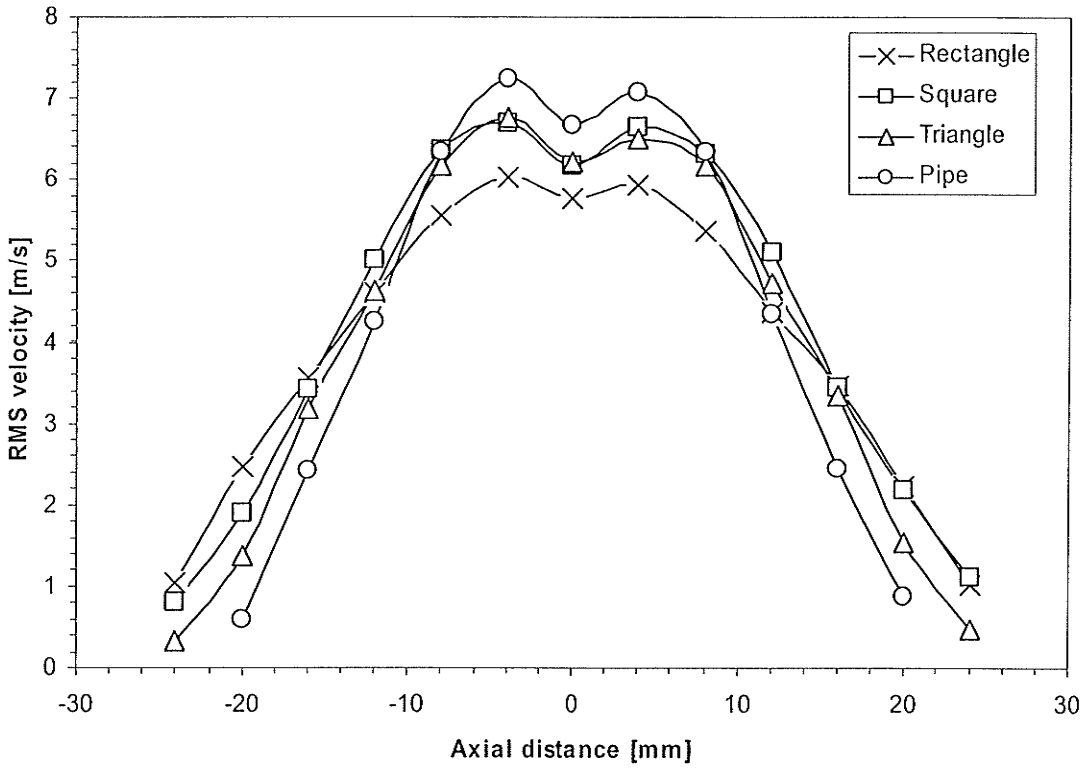

Figure 4.11: RMS velocity profiles at y = 103 *mm*

Figure 4.12 presents the non-dimensional rms centerline values for the square, triangular, rectangular and pipes nozzles. In this figure U_{cl} refers to the centerline velocity. The same figure is also used to compare our results with those of Mi et *al.* [11], who studied a sharp edge equilateral triangular nozzle and a contoured circular nozzle. It can be seen from this figure that all the nozzles tested in the present study, as well as those of Mi et al. [11], had similar trends of the centerline rms profiles. The major difference is the 'hump' that occured around $y/D_e = 7.5$. Whereas Mi et *al.* [11] noticed this hump only for the isosceles triangular nozzle (not shown in the figure), it appears to exist for all asymmetric nozzles tested in the present study. In addition, the rms velocity profiles for the rectangular nozzle was slightly higher in the near as well as mid field, i.e. $y/D_e \leq 30$. This

may have been due to the fact that the rectangular nozzle had a much lower centreline mean-velocity. Mi et *al.* [11] suggested that the centreline rms velocities were a key factor in mixing. Although this may be true, the results obtained in the present investigation indicate that the rms velocities at the jet boundary may be more important for mixing.

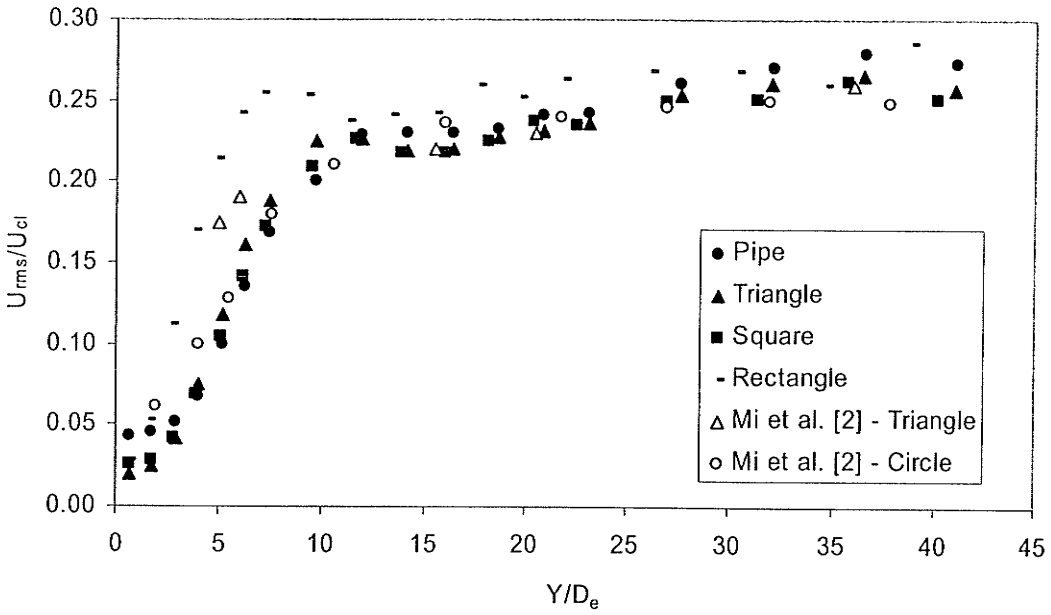

Figure 4.12: Non dimensional centerline normalized RMS profiles

4.3 Jet Methane Flame

The lift-off and flame height of methane jet flame expelling into still air have been determined for the rectangular, square, triangular, circular and pipe nozzles. The focus of this part of the study is on the effect of nozzle geometry on the jet flame lift-off and to a less extent, the flame length (or height).

4.3.1 Jet flame lift-off

For each experiment a total of around 2000 images of jet methane flames were taken of a given nozzle geometry by using a high speed camera. Note that the relatively high number of images was chosen to statistically improve the accuracy of the fluctuating flame length (height) and lift off. The height of each flame was measured from the nozzle exit plane. A MATLAB code was developed to analyse the images and determine the flame base based on the brightness of each pixel and then calculated the number of pixels between the nozzle exit and the flame base. The number of pixels was then multiplied by the pixel height to determine the lift off height. The imaging error was calculated by photographing a solid object of known height. The maximum error was found to be within 2%.

The lift-off height of each nozzle increases with the exit velocity as shown in Figure 4.13. This figure shows that the pipe nozzle tested in the present study had an identical lift-off to that of a smooth circular nozzle tested by Kalghati [24]. However, the same figure shows clearly that the asymmetrical nozzles' lift-off height was much lower than that of a

conventional pipe nozzle. The rectangular nozzle had the lowest lift-off height, followed by the triangular, square and finally circular nozzles. The lift-off height trend, for a given exit velocity, was inversely proportional to the axial RMS velocities near the nozzle exit. For example, the rectangular nozzle had the lowest lift-off height and the highest RMS velocity at the nozzle exit, followed by the triangular and square nozzles and finally the pipe. This suggests that the initial, or near field, entrainment and mixing were key factors in determining lift-off height.

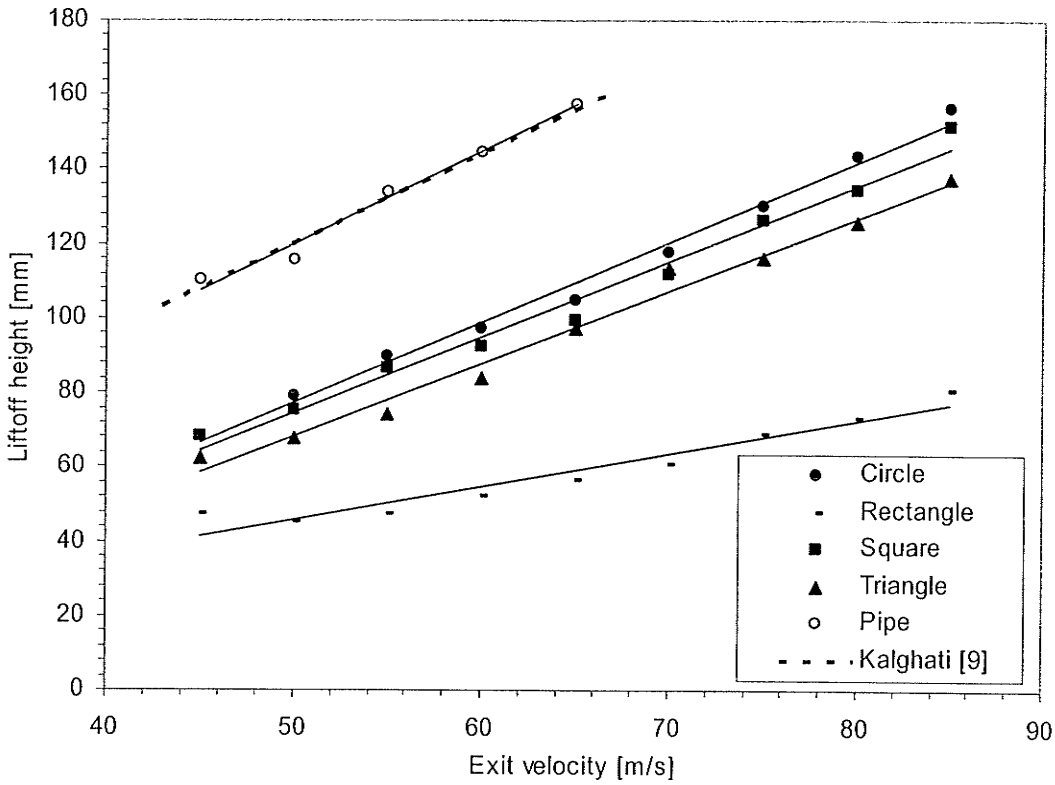

Figure 4.23: Lift-off height of methane jet flame for different asymmetric and conventional nozzles

Kalghati [24] proposed a non-dimensional lift-off empirical correlation for predicting the flame lift-off height, which was expressed as

$$\frac{hS_u}{\nu_e} = C\frac{U_e}{S_u}\left(\rho_e/\rho_\infty\right)^{1.5} \tag{4.2}$$

where h was the flame lift-off height, S_u was the laminar flame speed, ν_e was the kinematic viscosity of the fuel at the nozzle exit, U_e was the exit velocity of the fuel, C was a constant, ρ_e was the density of the fuel at the nozzle exit and ρ_∞ was the density of the ambient air. The values of these parameters are tabulated in Table 4.3.

Table 4.3. Values of the parameters in Equation (4.2)

S_u (m/s)	ν_e (m^2/s)	U_e (m/s)	ρ_e (kg/m^3)	ρ_∞ (kg/m^3)
0.39	1.75×10^{-5}	65	0.63	1.18

Kalghati [24] reported a value of $C = 50$ for all hydrocarbons issuing from round jets. For the present investigation, two different values of the constant C were determined for each nozzle and reported in Table 4.4. The values of C reported in the second column of Table 4.4 were obtained by using Equation (4.2) based on the assumption made by Kalghati [24], whereas the values in the second column were determined by using the original term $0.04 + 0.46(\rho_e/\rho_\infty) + 0.5(\rho_e/\rho_\infty)^2$ instead of the simplified term $(\rho_e/\rho_\infty)^{1.5}$. Kalghati [24] stated that his assumption were valid and provided accurate values of C within the range $0.5 < (\rho_e/\rho_\infty) < 2$. In the present investigation we found that ρ_e/ρ_∞ = 0.535 which was within the range reported by Kalghati [24]. However, as this value was near the limit of the range above, both methods were used to ensure accurate results. As

shown in Table 4.4, the approximated term $(\rho_e/\rho_\infty)^{1.5}$ produced a value of 0.391 while the original term produced a value of 0.429, which yields 8.8% difference between the original and approximated terms. However, when the approximated and original terms were used in equation 4.2 to determine the value of the constant *C*, the differences between the constants were much less as seen in Table 4.4. The difference seemed to be negligible and thus the approximation used by Kalghati [24] was adopted in order to compare the results of this study with those of Kalghati [24].

Table 4.4: Values of the constants *C* in the Equation (4.2)

Nozzle	C_1	C_2	Percent Difference*
Circular	34.30	33.44	2.5
Rectangular	18.76	18.28	2.6
Square	32.95	32.12	2.5
Triangular	30.45	29.68	2.5
Pipe	49.58	48.33	2.5
Kalghati [12]	50		

[1]used the $(\rho_e/\rho_\infty)^{1.5}$ term in the calculation

[2]used the $0.04+0.46(\rho_e/\rho_\infty)+0.5(\rho_e/\rho_\infty)^2$ term in the calculation

* $(C_1-C_2)/C_1 * 100$

Kalghati's [24] correlation was found to be valid only for the conventional pipe nozzle. However, for the asymmetrical nozzles the trend became exponential and had different values of the constant *C* as shown in Figure 4.14.

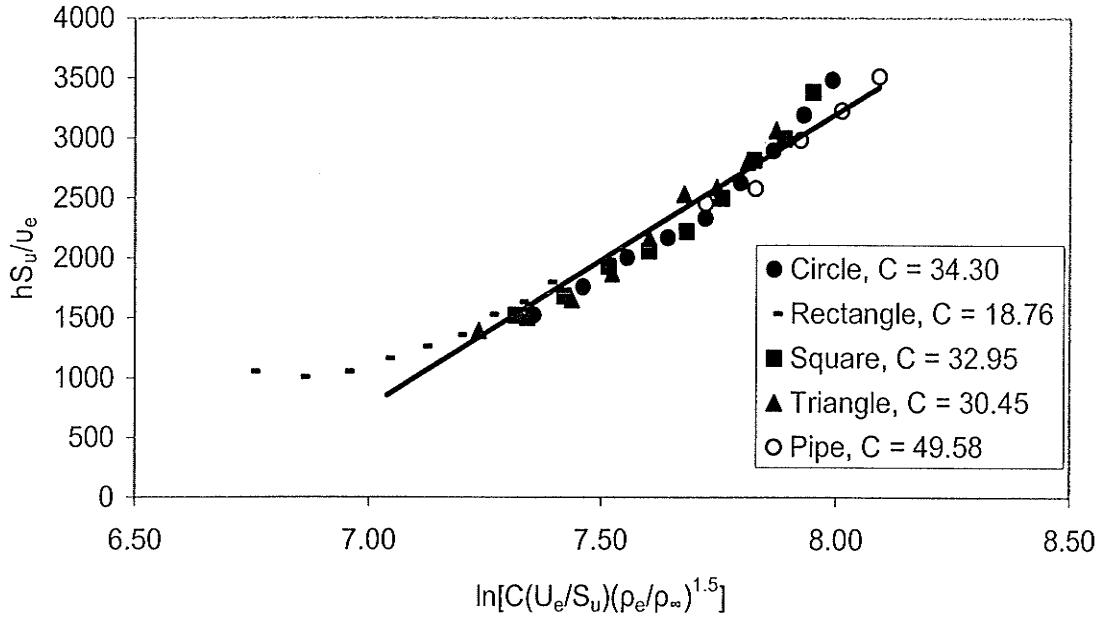

Figure 4.14: Kalghati's [24] non-dimensional jet flame lift-off height

A new correlation based on equation 4.2 and the jet decay from section 4.2.2 was developed as

$$\frac{hS_u}{\nu_e} \propto \ln\left[\frac{U_e}{S_u}\left(\rho_e/\rho_\infty\right)^{1.5}\left(U_{\max}/U_{cl}\right)^{4}\right] \tag{4.3}$$

This correlation is shown in figure 4.15. As centreline jet decay was found to be one of the factors associated with lift off height, the polynomial relationships for the centreline jet decay from Table 4.2 were coupled with Kalghati's [24] non dimensional lift off height equation. The new correlation describes the behaviour of all nozzles quite well. The triangular and rectangular nozzles fit very well with the relation while the pipe and square nozzles had a small error. An equation was determined using linear regression and is stated on the next page.

$$\frac{hS_u}{\nu_e} = 423.24 \ln\left[247.3 \frac{U_e}{S_u}\left(\rho_e / \rho_\infty\right)^{1.5}\left(U_{max} / U_{cl}\right)^4\right] - 1989.1 \qquad (4.4)$$

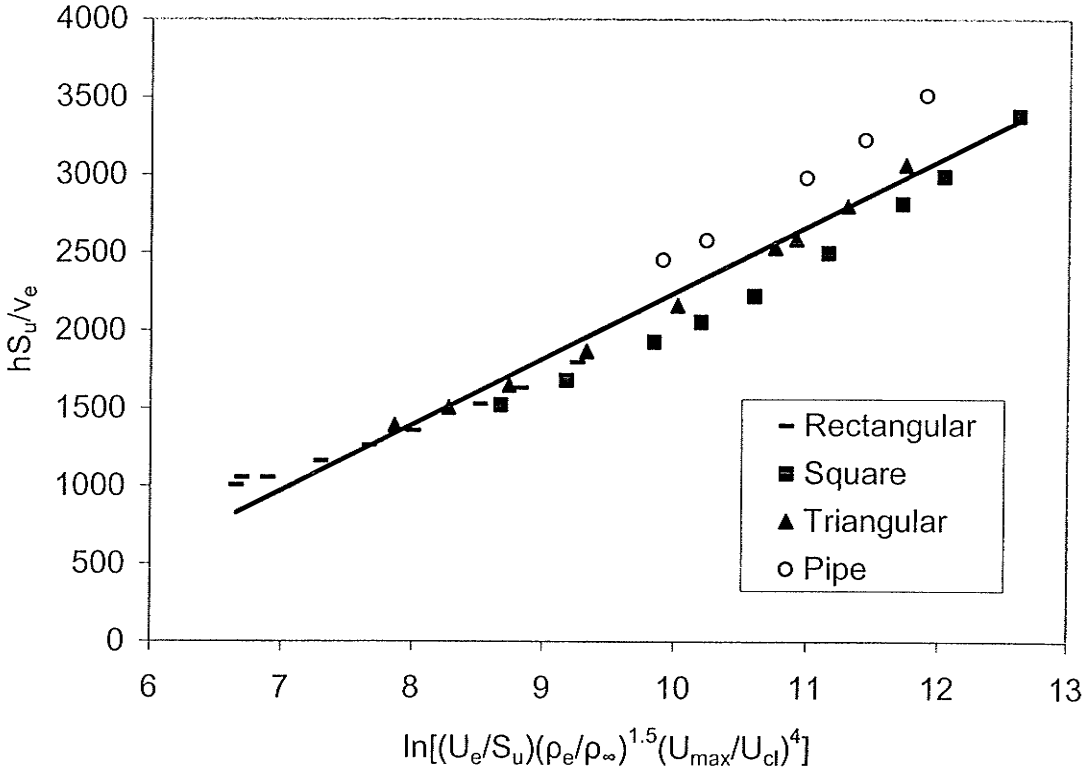

Figure 4.15: Proposed non dimensional jet flame lift-off height correlation

4.3.2 Jet flame height

The jet flame height (or length) was measured in the same manner as the lift-off height, with the only difference being that MATLAB code counted the number of pixels between the nozzle exit and the top of the flame. Approximately 2000 images were analysed for each experiment because it was found that the flame top fluctuates too much and thus requires a statistically large number of samples to determine an acceptable average value

of the flame length. As an example, the variation of the flame height for the square nozzle at a jet exit velocity of 75 *m/s* is shown in Figure 4.15 where it shows that the minimum and maximum flame heights are 59.50 *cm* and 121.46 *cm*, respectively, with a standard deviation of 9.01 *cm* which was an indication of large flame height fluctuations.

Becker and Liang [28] proposed an empirical correlation for predicting the non-dimensional flame heights represented by a non-dimensional grouping number ψ versus Richardson number ξ. These numbers were expressed, respectively, as

$$\psi = \left(\frac{D_s \beta}{L W_1} \right)^{2/3} \tag{4.5}$$

$$\xi = \left(\frac{g}{D_s^2 U_e^2} \right)^{1/3} L \tag{4.6}$$

where β was a constant for a given gas, L was the flame length, W_1 was the stoichiometric mass fraction of fuel [28] and D_s was given by

$$D_s = d_e (\rho_e / \rho_\infty)^{0.5} \tag{4.7}$$

where d_e was the burner exit diameter. The properties of methane and the nozzle equivalent diameters are reported in Table 4.5 and Table 4.6, respectively.

Table 4.5: Properties of methane

B	W_f	g [m/s^2]	S_u [m/s]
3.1	0.0549	9.81	0.39

Table 4.6: Equivalent nozzle diameters

Nozzle	Circle	Rectangular	Square	Triangular	Pipe
Equivalent Diameter [mm]	4.82	4.71	4.56	4.46	4.45

Figure 4.16 shows the non-dimensional flame height of the nozzles reported in Table 4.6. The same figure includes also the non-dimensional flame height of the pipe nozzle tested by Kalghati [24], who measured the flame length by averaging three photographs. Both ours and Kalghati's results were compared with the correlation proposed by Becker and Liang [28] who measured the flame length as the furthest downstream point at which the flaming gas was seen to dwell at an appreciable frequency. From Figure 4.16, the following observations were drawn. For a $\xi < 6$ our data over-predicted ψ, while the data of both Kalghati [24] and Becker and Liang [28] reasonably agreed. It was important to notice here that Kalghati averaged only three images to determine the flame height, which may have been a factor in the observed disagreement with our data in the range $\xi <$ 6. However, for a $\xi > 6$ our data seemed to agree with that of Kalghati [24] but still over-predicted ψ as reported by Becker and Liang [28], which may have been due to the difference in the definition of the flame height adopted by different authors.

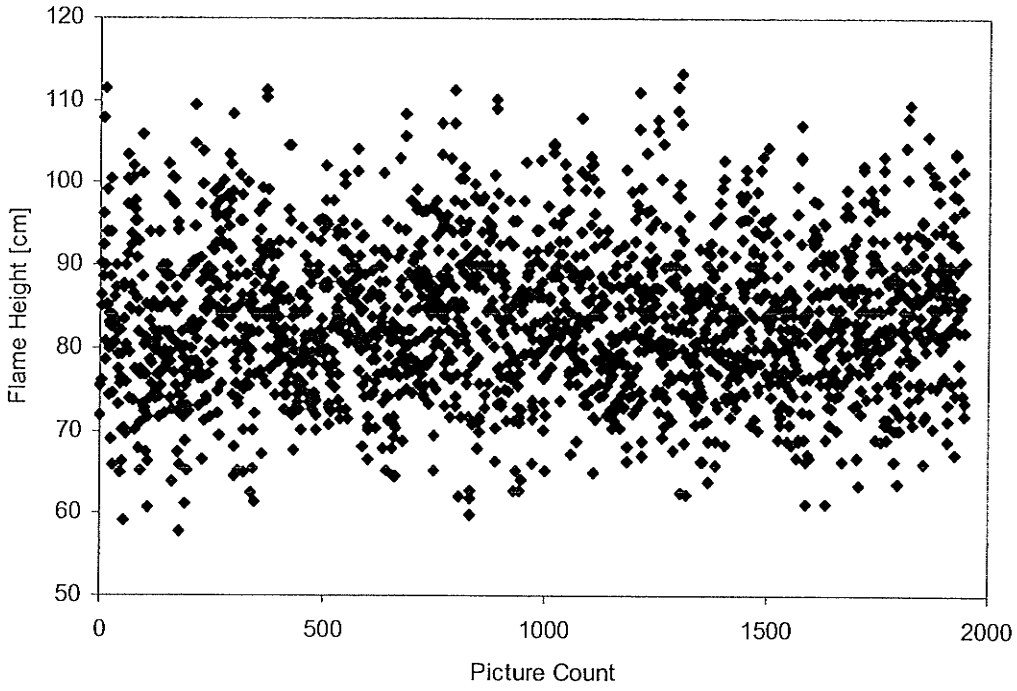

Figure 4.15: Height histogram for the square nozzle at a velocity of 75 *m/s*

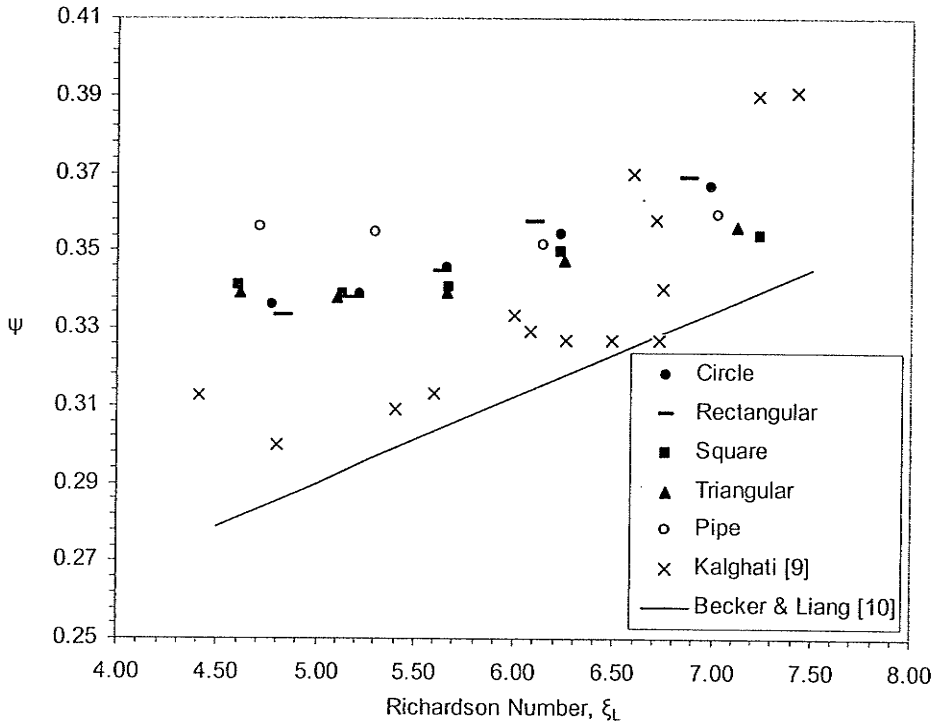

Figure 4.16: Non-dimensional flame height

4.4 Swirling Diffusion Methane Flame

The flame blow-out and stability of swirling diffusion methane flame issuing from asymmetric nozzles are presented and discussed in this section. This includes the flame shape and the blow-out limits for attached as well as lifted flames for various swirl numbers.

4.4.1 Shape of turbulent diffusion flame

Three different shapes of turbulent methane flame with zero-swirl co-flowing air were observed as shown in Figure 4.18 and their experimental conditions are displayed in Table 4.7. A long slender flame which was named CFA1, an edge flame called CFA2 and a highly lifted flame that was called CFA3. There was a fourth type of flame similar to that of CFA2 where the flame flickers, but it only existed for the triangular and square nozzles which will be explained later.

For the case of low swirl (i.e. S = 0.31) turbulent methane flow, three distinct flame shapes were observed; an attached cylindrical flame, a lifted bowl shape flame and an erratic lifted flame similar to CFA2 but much shorter. These flames were denoted CFB1, CFB2 and CFB3, respectively, as shown in Figure 4.18. The experimental conditions of these flames are displayed in Table 4.7.

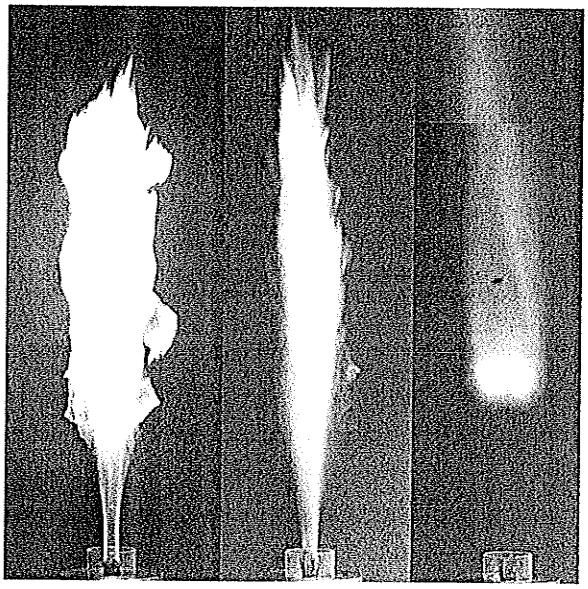

CFA1 CFA2 CFA3

Fig.4.17: Shapes of turbulent methane flame with co-flowing air having a zero-swirl

Although flame shapes with relatively high swirl number of co-flowing air ($S \geq 0.79$) were somewhat similar to those with relatively low swirl number ($S < 0.30$), four distinct flame types were observed as can be seen in Figure 4.19 with their experimental conditions reported in Table 4.7. The first one was an attached flame similar to CFB3 flame and the second was a highly erratic flame similar to CFB1 flame and thus it is denoted accordingly. However, the third one was an attached cone shaped flame with a blue bottom and an orange top, which was called CFC1. The fourth type of flames was an exception to the statement that flame shape is dictated by the swirl strength. We found that this flame shape depended also on the nozzle geometry. For the asymmetric nozzles, a slightly lifted, large based blue with top orange flame occurred, which is denoted CFC2.

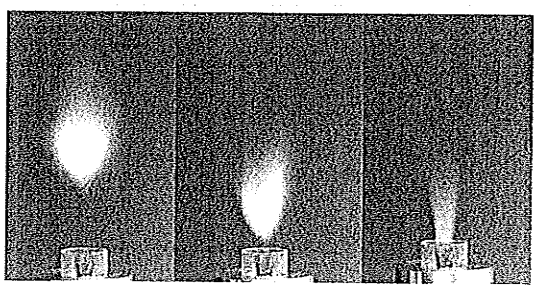

CFB1 CFB2 CFB3

Fig.4.18: Turbulent methane flame with co-flowing air having a swirl number $S = 0.31$

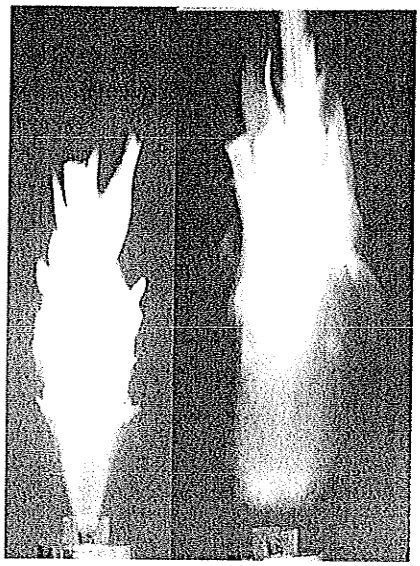

CFC1 CFC2

Fig.4.19. Turbulent methane flame with co-flowing air having a swirl $S \geq 0.79$ and $V_a \leq 5.71$ m/s

Table 4.7: Summary of various flame types and their experimental conditions

Flame type	Swirl Number, S	$\dot{m}_f \left(\frac{g}{s}\right)$	$\dot{m}_a \left(\frac{g}{s}\right)$	Nozzles
CFA1	0	0.087	5.97	All
CFA2	0	0.241	18.6	All
CFA3	0	0.303	6.24	All
CFB1	0.31	0.097	32.8	All
CFB2	0.31	0.197	26.7	All
CFB3	0.31	0.328	20.9	All
CFB1	0.79	0.359	29.9	All
CFB3	0.79	0.056	32.8	All
CFC1	0.79	0.197	11.9	All
CFC2	0.79	0.623	11.9	All
CFB1	1.15	0.390	29.9	All
CFB3	1.15	0.246	32.8	All
CFC1	1.15	0.246	12.5	Asymmetric
CFC2	1.15	0.087	5.97	Asymmetric

The results presented in this section clearly indicate that the flame shape was almost entirely dependant on the swirl strength and had very little reliance on nozzle shape. There were three exceptions, the CFC1, CFC2 and the pilot flame, which will be discussed later, but overall this statement holds true.

4.4.2 Blow-out limits of attached flames

Figure 4.20 shows the effects of fuel nozzle geometry on the blow-out limits of a non-swirling methane flame (i.e. the annular co-flow air has a zero-swirl, $S = 0$). The flame for each nozzle shape existed only below the corresponding curve shown in this figure. This figure shows that the blow-out limits of the flames issuing from the circular, triangular and square nozzles had similar trends. However, among these three flames, the circular nozzle had the lowest blow-out velocity and the square nozzle had the highest blow-out velocity. The rectangular nozzle's flame blow-out limits lied between those of the circular and triangular nozzles up to a fuel velocity of about 6.3 m/s. Beyond this velocity, the rectangular nozzle flame blow-out limits became higher than that of the triangular for $V_f > 6.3$ m/s, and the circular for $V_f > 7$ m/s. Finally, the flame blow-out limits for the circular and rectangular nozzles were exactly the same for $V_f < 2.4$ m/s; however, only the flame issuing from the rectangular nozzle existed for V_f higher than 8 m/s.

The fact that the circular nozzle had the lowest blow-out limit may be attributed to its weak spreading and mixing rate compared to the other two asymmetric jets (i.e. the square and rectangle). The highest blow-out velocity shown by the square nozzle was slightly unexpected as Mi et *al.* [11] had shown that triangular nozzles had the best mixing characteristics. The discrepancy may be caused by combustion which can alter turbulence characteristics and hence the mixing processes. Note that Mi et *al.*'s [11] studies were performed in still surroundings.

Another interesting phenomenon occurred for a flame with co-flowing air having zero swirl. For the square and triangular nozzles, a small attached flame formed and created a "pilot look-like" flame as the larger flame flickered at high fuel velocity (V_f above 5.8 *mls*). This flickering flame was a very small flame that was attached to the mouth of the fuel quarl and acted like a pilot flame. This "looks like" pilot flame was in turn attached to a much larger flame above it, which extinguished and reignited every second or so. This flame accounted for the negative slope for the triangular and square nozzles as can be seen in Figure 4.20.

For the highest swirl number tested in the present experiment, i.e. S = 1.15, the flame blow-out occurred at low fuel velocities (depending on the nozzle shape) as shown in Figure 4.21. Recall that each flame existed below its corresponding curve displayed in Figure 4.21. It was important to note that the maximum air velocity that could be reached in the present study was V_a = 11.41 m/s, therefore, flame blow-out limits beyond this velocity were not been explored here. Figure 4.21 shows that at a fuel velocity below V_f = 1.40 m/s, the flame blow-out conditions were similar for all the tested nozzles because of the extremely erratic nature of the flame. However, beyond $V_f \sim$ 1.4 m/s, Figure 4.21 shows that for any given V_f the square and triangular nozzles stabilized the flame at the highest airflow velocity followed by the rectangular and finally the circular nozzle. In addition, Figure 4.21 shows that the asymmetric nozzles appeared to follow a linear flame blow-out relationship between the airflow exit velocity, V_a, and the fuel exit velocity, V_f, while the circular nozzle began with a linear relationship and then deviated at fuel velocity above 2 m/s.

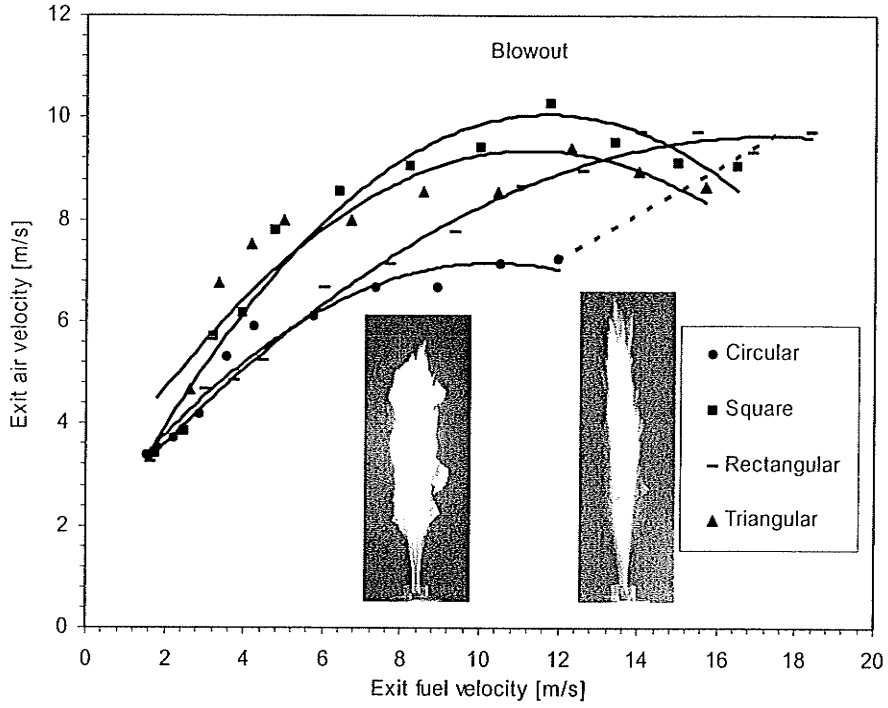

Figure 4.20: Blow out the attached laminar and unstable pilot flames for various nozzles at $S = 0$

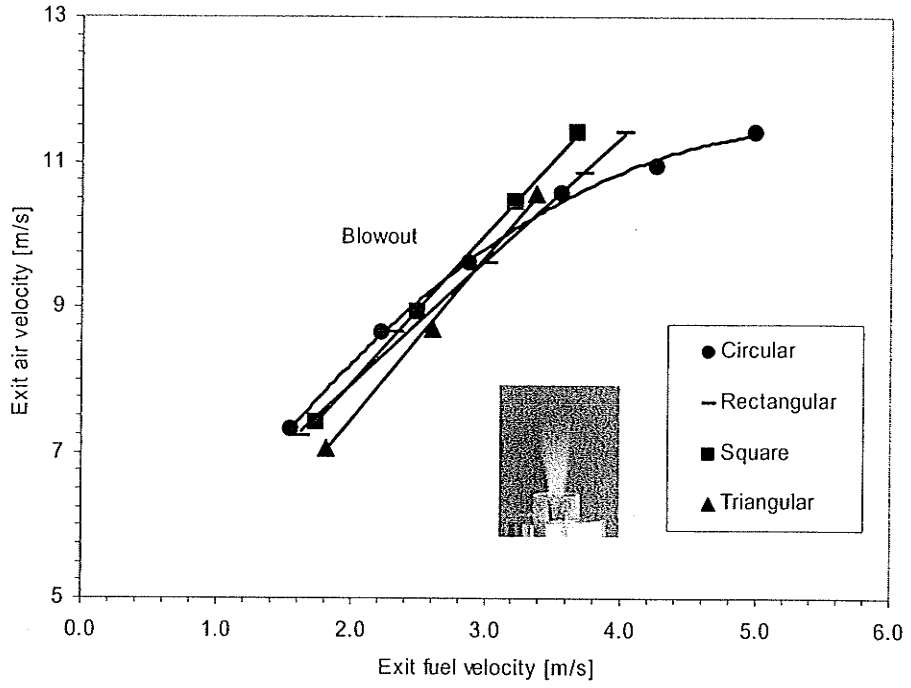

Figure 4.21: Blow out of the attached conical flame for various nozzles at S =1.15

4.4.3 Blow-out limits of lifted flames

Figure 4.22 shows that for the case of zero-swirl, co-flowing air, the blow-out for highly lifted turbulent flames appeared to be independent of the nozzle shape. Note that the flame existed only below the curves seen in Figure 4.22, but the flame may have been stable at $V_f > 18.41$ m/s, which was the maximum fuel velocity reached in the present experiment. In addition, for all the tested four nozzles, Figure 4.22 shows that the flame blow-out pattern followed a linear relationship between the air flow and fuel flow exit velocities. This was caused mainly by the extremely high liftoff of the flame. By the time the fuel jet had reached the flame base, the jet structure mixed with the swirling co-flow air. It seemed that the stoichiometric ratio of fuel to air was the main factor behind flame stability in this case.

For a relatively weak swirl, i.e. $S = 0.31$, the four nozzles had similar flame blow-out characteristics but there were slight differences as can be seen in Figure 4.23. Each flame existed below its corresponding curve displayed in Figure 4.23. These blow-out limits, indicated by the curves in this figure, may have increased if the air velocity increased beyond its maximum value attainted in the present experiment. In addition, this figure shows that at low fuel velocities, below $V_f = 6.40$ m/s, the triangular nozzle had the best flame stability (i.e. blew-out at a relatively higher air velocity), followed by the rectangular, square and finally the circular nozzle. This seemed to be consistent with the findings of Mi et *al.* [11] who studied the mixing characteristics of a jet airflow issuing from different asymmetric nozzles in still air. The results of the present cold flow study indicated that the rectangular nozzle would have the best mixing characteristics. The

discrepancy may have been due to the changes in the flow properties caused by the swirl. In the case of swirling co-airflow, the recirculation zone was believed to have much slower velocities and was more alike to that of still air than a zero-swirl which could have explained the similar trends compared to those of Mi et *al.* [11]. However, based on our observations, it was believed that as the air velocity increased (beyond V_a = 6.40 m/s), so did the strength of the recirculation zone as the flame was in less and less of a region that resembled still air. Moreover, Figure 4.23 reveals that the trend for the most stable flame, based on blow-out limit, which occurred for the triangular nozzle, begins to deviate slightly at these higher air velocities (beyond V_a = 6.40 m/s). Nevertheless, the flame blow-out conditions for all the nozzles were quite similar, although not as similar as to those for the zero-swirl flames blow-out limits, which are presented in Figure 4.21. It is believed that this was caused by the flame liftoff which was smaller for the swirling flames compared to that of the non-swirling flames.

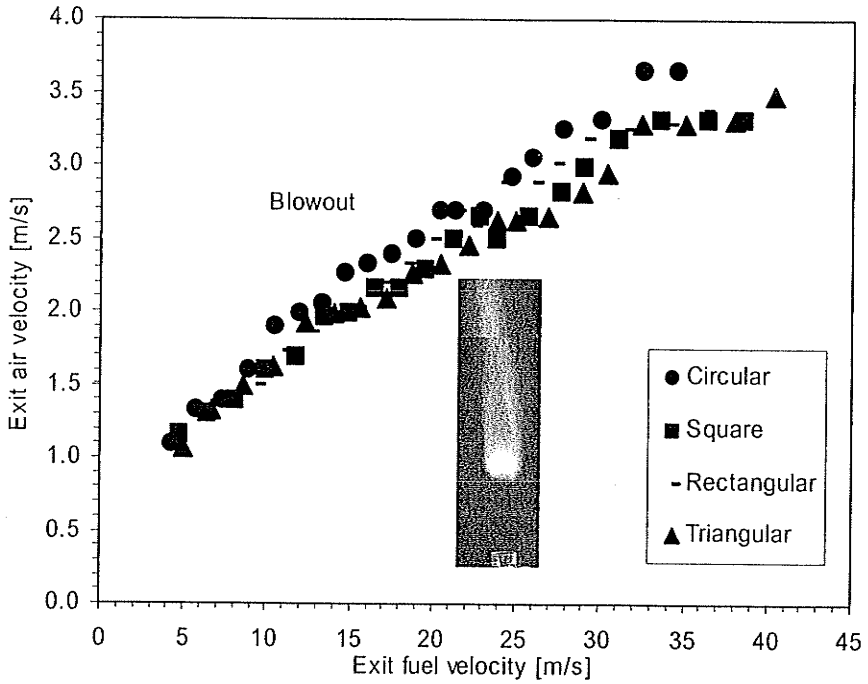

Figure 4.22: Blow out of the highly lifted flame for various nozzles at S = 0.31

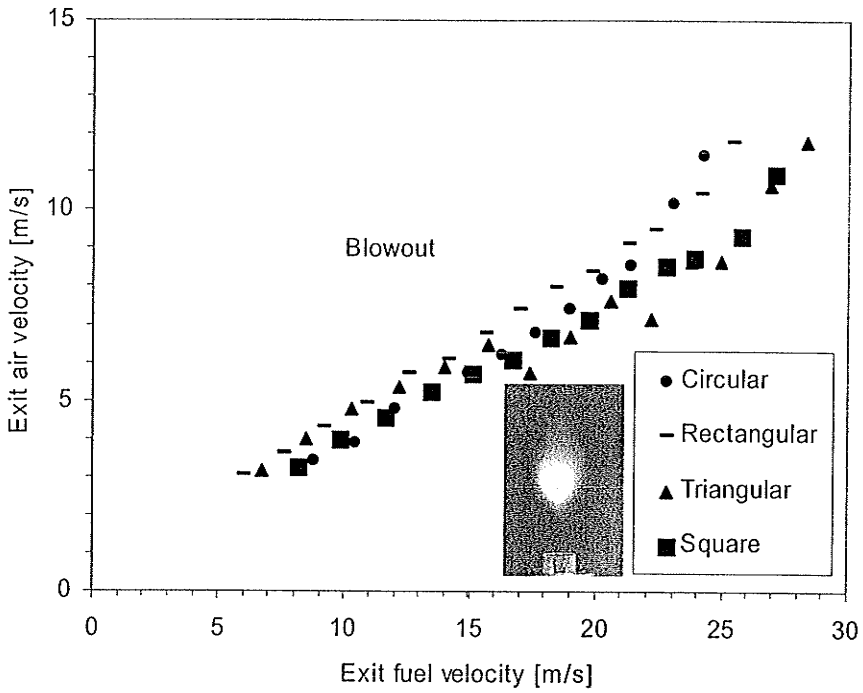

Figure 4.23: Blow out of the lifted erratic flame for various nozzles at S = 0.31

Chapter 5: Conclusions and Recommended Future Work

5.1 Introduction

This chapter summarizes and discusses briefly the major findings achieved in this research. It will also discuss improvements that can be made to the existing experimental setup. Finally, recommended future work is outlined.

5.2 Discussion of the Major Findings

The major findings of this study concern the effect of asymmetrical nozzles on the flow behavior downstream of the nozzle exit. Studies were performed to assess the effect of nozzle geometry on (i) the jet cold flow mean-velocity and turbulence intensity profiles on the centreline of the jet, (ii) the jet methane flame lift-off and height and (iii) the shape and blow-out limits of swirling diffusion methane flame.

The measured jet flame liftoff height for the asymmetrical nozzles seemed to have a correlation with the jet turbulence intensities. Out of the different nozzles tested, the pipe nozzle had the highest jet flame lift-off height and the rectangular nozzle had the smallest lift-off height. Although the variation of the jet mean-velocity profiles appeared to correspond to that of the jet flame lift-off height for each nozzle, the turbulence intensities corresponded much better. The turbulence intensities for the asymmetric nozzles were much greater near the nozzle exit, which was an indication of a greater entrainment of ambient air into the jet stream, and suggested that once enough combustible air had mixed with the fuel, the flame could ignite and anchor itself at that

location. As the pipe had the lowest turbulence intensities, it would take longer to entrain the air and thus yields a higher lift-off. Further downstream of the nozzle exit (i.e. the far field), the turbulences intensities were quite similar for all the nozzles suggesting that the initial mixing was a key factor in determining lift-off height. This theory agreed with the findings of Kalghati [24] but refuted the findings of Upatnieks et *al.* [25] who found that turbulence intensity had little effect on the propagation speed of the flame's base. It should be noted that the results of Upatnieks et *al.* [25] were found for a Reynolds number of 8500. Also, Upatnieks et *al.* [25] recognized that his suggestion may not have been correct at higher Reynolds numbers, which was the case in the present study as well as in [24] where $Re \geq 15{,}000$. But it must be recognized that in both the present study and that in [24] the mean velocity and turbulence measurements were taken only for the cold flow and not in the presence of combustion, which can alter the flow field characteristics.

The stability of turbulent diffusion methane flame with co-airflow was shown to improve with asymmetrical nozzles. For the case of zero-swirl co-airflow, the attached flame could exist at much higher velocities compared to that with a conventional pipe nozzle.

5.3 Improvements of the Experimental Setup

The following improvements of the burner test rig are suggested:

(a) Alignment of the central nozzle is required in order to ensure its alignment with the co-airflow.

(b) Ensure perfect seal of the burner to avoid any gas or air leakages.

(c) Improve the design of the seeder for the gas flow in order to increase the seeding particles concentration in the gas flow. The seeder design should be improved to incorporate a sort of cyclone to force the flow to rotate and hence pick up more particles

(d) Presently, the volumetric airflow was limited to 600 *LPM*. Therefore, additional air supply is required to expand the co-airflow velocity range, which then will help to determine the entire flame stability limits.

(e) The measurements of the flame height were also restricted by the height of the overhead exhaust hood. Measurements at high velocities could not be taken because of interference from the hood. If the hood was raised, a broader range of measurements could be taken.

(f) A second dimension to the LDA system should be incorporated to characterize better the jet and swirling flows. As swirling flow has a large tangential component, the two dimensional LDA would give a much better understanding of the entire flow field.

5.4 Recommended Future Work

The following suggestions are recommended for further future work:

(*i*) Characterize the jet and swirling flows with and without flame in two planes, that is, along the two vertical orthogonal planes, *z-x* and z-*y*. The LDA measurements in the presence of flame would be extremely beneficial to confirm or deny the assumption of the cold flow being similar to the reactive case.

(*ii*) The use of Particle Image Velocimetry (PIV) to map instantaneously the flow field would help determine better the flow recirculation zones. PIV can also be used to characterize the mixing process downstream of the nozzle.

(iii) Determine the effect of nozzle shape on jet flame blow out limits in an attempt to correlate this data with previous studies on circular nozzles. An increased blow out limit will result in a more stable flame under a wider range of flow conditions.

References

[1] The International Workshop on Measurements and Computation of Turbulent Nonpremixed Flames, Sandia National Laboratories, CA, USA: www.ca.sandia.gov/tdf/Workshop.html.

[2] Kalt, P.A.M., Al-Abdeli, Y.M., Masri, A.R., and Barlow, R. S., Swirling turbulent non-premixed flames of methane: Flow field and compositional structure, *Proceedings of the Combustion Institute* 29 (2002) 1913-1919.

[3] Masri, A.R., Kalt, P.A.M. and Barlow, R.S., The compositional structure of swirl-stablised turbulent nonpremixed flames, *Combustion and Flame* 137 (2002) 1-37

[4] Kim, S-H, Kim, M., Yoon, Y. and Jeung, I-S., The Effect of Flame Radiation on the Scaling of Nitrogen Oxide Emissions in Turbulent Hydrogen Non-Premixed Flames, *Proceedings of the Combustion Institute* 29 (2002) 1951-1956

[5] Dally, B.B., Karpetis, A.N. and Barlow, R.S., Structure of Turbulent Non-Premixed Jet Flames in a Diluted Hot Coflow, *Proceedings of the Combustion Institute* 29 (2002) 1147-1154.

[6] Zhou, L.X., Chen, X.L. and Zhang, J., Studies on the Effect of Swirl on NO Formation in Methane/Air Turbulent Combustion, *Proceedings of the Combustion Institute* 29 (2002) 2235-2242

[7] Schmittel, P., Gunther, B., Lenze, B., Leuckel, W. and Bockhorn, H., Turbulent Swirling Flames: Experimental Investigation of the Flow Field and Formation of Nitrogen Oxide, *Proceedings of the Combustion Institute* 28 (2000) 303-309

[8] Chen, R-H. and Driscoll, J.F., The Role of the Recirculation Vortex in Improving Fuel-Air Mixing withing Swirling Flames, *22nd Symposium on Combustion* (1988) 531-540

[9] Quinn, W.R. On the mixing in an elliptical turbulent free jet, *Physics of Fluids* A1 (1989) 1716-1722.

[10] Quinn W.R. Measurements in the near flow field of an isosceles triangular free jet, *Experiments in fluids* 39 (2005) 111-126.

[11] Mi, J., Nathan, G. J., Luxton, R. E. Centreline Mixing Characteristics of Jets from Nine Differently Shaped Nozzles, *Experiments in Fluids* Vol 28, 2000, pp. 93-94.

[12] S.R. Gollahalli, T. Khanna, and N. Prabhu, Diffusion Flames of Gas Jets Issued from Circular and Elliptic Nozzles, Comb. *Sci. and Tech. Journal* 86 (1992) 267-288.

[13] N. Prabhu, S.R. Gollahalli, Effect of Aspect Ratio on Combustion Characteristics of Elliptic Nozzle Flames, *Emerging Energy Technology, ASME PD* 36 (1991) 51-56.

[14] A. Kamal, S.R. Gollahalli, Effects of Jet Reynolds Number on the Performance of Axisymmetric and Nonaxisymmetric Gas Burner Flames, *Journal of Energy Resources Technology, ASME* 123 (2001) 167-172.

[15] K.C. Schadow, K.J. Wilson, M.J. Lee and E. Gutmark, Enhancement of Mixing in Ducted Rockets with Elliptic Gas-Generator Nozzles, *20th Joint propulsion Conference*, Ohio, AIAA Paper 84-1260 (1984).

[16] E. Gutmark, K.C. Schadow, and K.J. Wilson, Subsonic and Supersonic Combustion Using Noncircular Injectors. *Journal of Propulsion* 27 (1991) 240-249.

[17] N. Papanikolaou, I. Wierzba, The Effects of Burner Geometry and Fuel Composition on the Stability of a Jet Diffusion Flame, *Journal of Energy Resources Technology* 119 (1997) 265-270.

[18] N. Papanikolaou, I. Wierzba, An Experimental Investigation of the Effects of Nozzle Ellipticity on the Flow Structure of co-Flow Jet Diffusion Flames, *J. Braz. Soc. Mech. Sci.* 23 (2001) 1-13.

[19] Turns, S. An Introduction to Combustion. 2nd Ed, 2000.

[20] Wohl K., Gazley C., Kapp N. Diffusion Flames, *Third Symposium on Combustion and Flame and Explosion Phenomena.* Baltimore, MD (1949) 288.

[21] Vanquickenborne, L. & van Tiggelen, A. The Stabilization Mechanism of Lifted Diffusion Flames. *Combustion and Flame* 10 (1966).59-69.

[22] Peters, N. Local Quenching Due to Flame Stretch and Non-Premixed Turbulent Combustion, *Combustion Science and Technology* 30 (1983) 1-17.

[23] Broadwell, J.E., Dahm, W.J.A. & Mungal, M.G. Blowout of Turbulent Diffusion Flames, *20th Symposium (International) on Combustion* (1984) 303-310.

[24] Kalghati, G.T. Lift-off Heights and Visible Lengths of Vertical Turbulent Jet Diffusion Flames in Still Air. *Combustion Science and Technology* 41 (1984) 17-29.

[25] Upatnieks, A., Driscoll, J.F., Rasmussen, C.C. & Ceccio, S.L. Lift-off of turbulent jet flames-assessment of edge flame and other concepts using cinema-PIV, *Combustion and Flame* 138 (2004) 259-272.

[26] Kalghati, G.T. Blow-Out Stability of Gasesous Jet Diffusion Flames. Part I: In Still Air, *Combustion Science and Technology* 26 (1981) 233-239.

[27] Chao, Y-C., Wu, C-Y., Lee, K-Y., Li, Y-H., Chen, R-H & Cheng, T-S. Effects of Dilution on Blowout Limits of Turbulent Jet Flames, *Combustion and Flame* 176 (2004) 1735-1753.

[28] Becker, H.A. & Liang, D. Visible Length of Vertical Free Turbulent Diffusion Flames. *Combustion and Flame* 32 (1978) 115-137.

[29] Beer, J.M., Combustion Aerodynamics, London Applied Science Pulishers Ltd, 1972

[30] TSI LDV/PDPA System Instruction Manual, July 2001, Combustion Laboratory, Room E3-340 Engineering building, University of Manitoba, Winnipeg.